SYNTHETIC ANALOGS OF THE NON-HEME IRON CENTER IN SUPEROXIDE REDUCTASE

by

WREN HILLIARD CHEATUM

(Under the Direction of Todd C. Harrop)

ABSTRACT

Reactive oxygen species, such as superoxide, are associated with many diseases including cancer, diabetes, and atherosclerosis. In order to protect against the presence of reactive oxygen species, organisms have evolved mechanisms to detoxify superoxide mediated by the enzymes superoxide dismutase (SOD) and superoxide reductase (SOR). SOR is a non-heme iron enzyme present in anaerobic and microaerophilic biological systems that is utilized for the detoxification of superoxide via its one-electron reduction to form hydrogen peroxide. The present work describes the synthetic analogs of the active site of SOR through the utilization of neutral, nitrogenous ligands in combination with exogenous thiolate ligands about an iron center in order to mimic the histidine and cysteine residues of the enzyme. The varying nitrogenous ligands include pyridine and imidazole substituents as the nitrogen donor. The synthesis and characterization of theses model systems contributes to the understanding of the mechanism of SOR.

INDEX WORDS: Superoxide, Superoxide reductase, Non-heme iron, Bioinorganic chemistry, synthetic analog

SYNTHETIC ANALOGS OF THE NON-HEME IRON CENTER IN SUPEROXIDE REDUCTASER

by

WREN HILLIARD CHEATUM

B.S.CHEM., The University of Georgia, 2007

A Thesis Submitted to the Graduate Faculty of The University of Georgia in Partial Fulfillment
of the Requirements for the Degree

MASTER OF SCIENCE

ATHENS, GEORGIA

2009

SYNTHETIC ANALOGS OF THE NON-HEME IRON CENTER IN SUPEROXIDE REDUCTASE

by

WREN HILLIARD CHEATUM

Major Professor:	Todd C. Harrop
Committee:	Michael K. Johnson Michael W. Adams

Electronic Version Approved:

Maureen Grasso
Dean of the Graduate School
The University of Georgia
August 2009

ACKNOWLEDGEMENTS

This thesis would not have possible without the continued support and direction of my research advisor Professor Todd Harrop. Along with Professor Michael Johnson and Professor Michael Adams, Professor Harrop guided me through my journey with patience and understanding. Also, I would like to extend my sincere gratitude towards my fellow lab members: Eric Gale, Vivian Ezeh, and Koustub Dube. I would especially like to thank Dr. Ashis Patra for the helpful and thoughtful guidance through the completion of this thesis. Additionally I would like to thank various members of the chemistry department at the University of Georgia for their assistance in experiments including Dr. Dennis Philllips, Dr. Greg Wylie, and Dr. Pingrong Wei. This thesis is the product of many people's contributions, and I am deeply indebted to their support and assistance.

TABLE OF CONTENTS

Page

LIST OF TABLES

Page

LIST OF FIGURES

CHAPTER 1

INTRODUCTION

Reactive Oxygen Species

Reactive oxygen species (ROS) are highly reactive small molecules containing oxygen and are responsible for oxidative stress on biological organisms including both prokaryotes, such as *E. coli*, and more complex eukaryotic organisms, such as humans. Such ROS include hydrogen peroxide (H_2O_2), hydroxyl radical ($OH\cdot$), peroxynitrite ($OONO^-$), and superoxide ($O_2^{\bullet-}$). While these ROS are potentially harmful to organisms, they are naturally produced through normal metabolic processes.[1, 2] Specifically, four enzyme systems have been shown to be predominant in the production of ROS: NADPH oxidase, xanthine oxidase, uncoupled NO synthase, and the mitochondrial electron transport chain.[3, 4] For example, oxygen is reduced to $O_2^{\bullet-}$ using NADPH as the electron donor in NADPH oxidase aiding the defense system against microbial infection in leukocytes.[5] Since ROS are naturally occurring molecules, organisms have developed ways in which to utilize their presence. For instance, ROS have been shown to be employed as secondary messengers for different cytokines and growth factors.[6, 7] ROS have also been shown to be produced in the signaling pathways of apoptosis regulation.[8, 9] However, an excess of ROS leads to more detrimental circumstances for an organism. Oxidative stress leads to damage of proteins, lipids, lipoproteins, DNA and other cellular components.[10-12] ROS have been associated with diseases such as hypertension, diabetes, and atherosclerosis as well as aging.[13-18] For example, studies have demonstrated that the superoxide anion ($O_2^{\bullet-}$) is responsible for endothelial dysfunction by inactivating the vasodilator nitric oxide (NO), the endothelium-derived relaxing factor, leading to cardiovascular disease.[19] Superoxide reacts with NO to form peroxynitrite ($OONO^-$), a powerful cytotoxic oxidant which is capable of causing oxidative stress to biological media through protein nitration.[20] In addition to being formed through natural metabolic processes, superoxide is also generated through the spontaneous one-electron reduction of free molecular oxygen, and this may take place in aerobic environments.[4] Since superoxide and other ROS are such detrimental small molecules in the biological milieu, organisms have devised methods of detoxifying ROS present in the cell and extracellular space through the use of metalloenzymes.

Detoxification of ROS

Organisms have devised defense systems to extract the reactive oxygen species from inflicting significant oxidative damage in order to protect the organism. The detoxification of ROS is accomplished with enzymes capable of redox reactions utilizing transition metal centers. These enzymes convert ROS to species which are either chemically benign to the organism or can be further detoxified. For instance, the presence of H_2O_2 causes oxidative stress and is counteracted by catalases and peroxidases as shown in equations 1 and 2. These enzymes convert H_2O_2 to molecular oxygen and water depending upon the requirement of the organism.

$$2H_2O_2 \xrightarrow{\text{catalase}} 2H_2O + O_2 \qquad (1)$$

$$H_2O_2 + RH_2 \xrightarrow{\text{peroxidase}} 2H_2O + R \qquad (2)$$

Other enzymes contain metal ions which assist in the detoxification of superoxide. Since superoxide is a naturally occurring product of aerobic metabolism, aerobic organisms utilize superoxide dismutases (SOD) that destroy superoxide by disproportionating it to hydrogen peroxide and molecular oxygen (eq 3).[21] The corresponding hydrogen peroxide product is further detoxified by catalase enzymes (eq 1).[22] SOD catalyzes both the oxidation and the reduction of superoxide and operates utilizing both by cycling through the reduced and oxidized forms of the catalytic metal center.

$$2O_2^{\bullet -} + 2H^+ \xrightarrow{\text{SOD}} H_2O_2 + O_2 \tag{3}$$

The dismutation of superoxide occurs at a redox-active metal site. To date, there are four different types of SOD enzymes found in various aerobic organisms. One such enzyme is the SOD containing a catalytically-active copper ion as well as a zinc ion that does not contribute to catalysis at the active site present in the cytosol of eukaryotic cells.[21, 23] Another SOD enzyme contains nickel at the active site and is present in certain fungi and bacteria.[24] A third type of SOD enzyme contains either iron or manganese in structurally similar active sites.[25] While these enzymes all catalyze the disproportionation reaction, the mechanism whereby this reaction occurs is slightly different for each.

Superoxide Reductase

While the concentration of molecular oxygen is significantly less in microaerophilic environments (2.5-5% O_2)[26] and essentially absent in anaerobic environments when compared with the atmosphere (21% O_2),[25] metabolic processes can continue to produce superoxide with the minor amount of oxygen present which could lead to oxidative stress.[27, 28] The presence of superoxide in microaerophilic and anaerobic organisms requires a mechanism to remove the superoxide present without producing molecular oxygen, which would be detrimental to the organism. Such organisms have developed a non-heme iron enzyme, superoxide reductase (SOR) which does such a task and selectively reduces superoxide to hydrogen peroxide without the accumulation of dioxygen as shown in equation 4.[27, 29-32] The H_2O_2 product is further detoxified by peroxidase enzymes preventing any formation of molecular oxygen (eq 2).[22, 33]

$$O_2^{\bullet -} + 2H^+ + e^- \xrightarrow{SOR} H_2O_2 \qquad (4)$$

The X-ray crystallographic structure of both the reduced and the oxidized form of SOR from *Pyrococcus furiosus* has been reported by Rees and coworkers.[34] SOR is a homotetramer (14 kDa) consisting of four subunits with one iron present in each subunit as shown in Figure 1.1. The crystal structure of *P. furisosus*, as well as the 2Fe-SOR (vide infra) crystal structure in *Desulfovibrio desulfuricans*,[35] reveals that this iron ion is the site at which the reduction of superoxide occurs. In the reduced form of the enzyme (SOR_{red}), the high-spin ferrous ion ($S = 2$) is bound to four histidine residues in the equatorial plane and a cysteine residue resulting in a square-pyramidal coordination geometry. The oxidized form of SOR (SOR_{ox}) comprises a distorted octahedral geometry with the addition of a glutamate-O ligand *trans* to the cysteine ligand about the Fe^{3+} center.[34, 36] SOR contains the necessary structural properties to selectively detoxify superoxide via reduction. The active site is located at the periphery of the protein where it is readily exposed to solvent (e.g. potential proton source) and easily accessible for superoxide to bind to the iron ion. In contrast to the 1Fe-SOR present in *P. furiosus*, there is another type of SOR enzyme discovered in *Desulfovibrio vulgaris* which contains an additional iron site in the protein, termed 2Fe-SOR.[37] This iron is bound to four cysteine residues similar to rubredoxin, and the function of this second iron site is not yet known due to the continuous enzyme activity and analogous spectroscopic properties upon mutation of the $[Fe(SCys)_4]$ site.[38, 39] The $[Fe(NHis)_4(SCys)]$ site of the 2Fe-SOR is structurally similar to that of the 1Fe-SOR.[35]

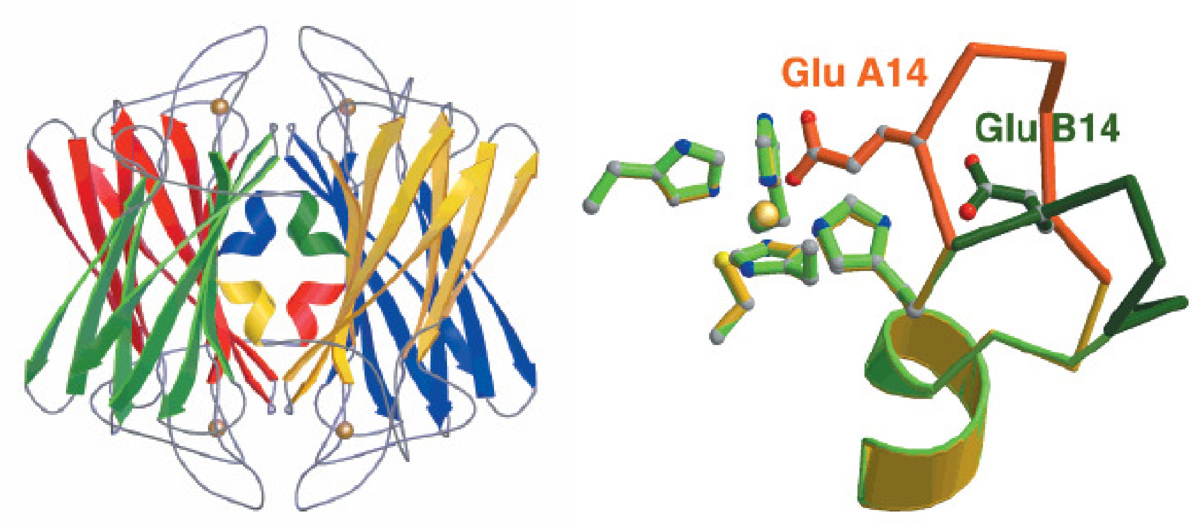

Figure 1.1. The SOR enzyme isolated from *P. furiosus*. (Left) Ribbon diagram of the homotetrameric arrangement of SOR with the spheres depicting the iron atoms. (Right) The oxidized (indicated by orange glutamine residue) and the reduced (dark green) forms of the active site of SOR.[34]

The bond distances of the ligands bound to the iron center in *P. furiosus* are shown in Table 1.1. The length of the Fe-SCys in the active site of SOR (2.44 Å) is longer than the typical iron-sulfur bond which is approximately 2.3 Å when in a similar square-pyramidal geometry with nitrogen-containing ligands in the equatorial plane.[40] The longer distance of the (Cys)S-Fe bond is proposed to be a factor in the cleavage of the Fe-O bond as a result of the high-spin iron ion, as opposed to the cleavage of the O-O bond as in heme-containing and structurally similar cytochrome P450.[41] According to DFT calculations, the hydrogen bonding to the thiolate ligand from peptide N-H of nearby isoleucine and asparagine residues in the secondary coordination sphere causes this elongation of the Fe-S bond.[34, 42] Additionally, the exposure of the iron site to solvent allows for more accessible protons to form the hydroperoxo intermediate resulting in the release of hydrogen peroxide.

Table 1.1. Fe-L distances (in Å) in the oxidized and reduced forms of SOR subunits in *P. furiosus*. The ranges indicated are the varying bond distances of the different subunits.[34]

Ligand	Oxidized SOR (Å)	Reduced SOR[a] (Å)
His 16	2.09-2.13	1.97-2.7
His 41	2.17-2.24	2.26-3.1
His 47	1.99-2.16	1.9-2.13
His 114	2.16-2.20	2.0-2.2
Cys 111	2.46-2.68	2.40-2.7
Glu 14	2.57-2.59	-

[a] The bond distances reported with lower precision values are less accurate due to lower Fe occupancies at the respective sites.

The reaction catalyzed by SOR involves the selective one-electron and proton-assisted reduction of superoxide to selectively form hydrogen peroxide at a diffusion-controlled rate (Scheme 1.1).[43] This reaction is essentially the reducing half-reaction of the SOD mechanism and does not form molecular oxygen which would be detrimental to the anaerobic organism. The axial glutamate ligand bound to the iron atom in SOR_{ox} acts as a "gate" for the enzyme. This binding of the glutamate ligand is proposed to be one of the reasons why SOR only performs the reductive half-reaction of SOD and not the oxidation of superoxide as the coordination sphere becomes saturated, and the Fe^{3+} center becomes difficult to re-reduce by superoxide.[33] The proposed mechanism contains a hydroperoxo intermediate.[44] The oxidized form of the enzyme, termed the "resting ferric" state, is bound to the glutamate ligand in the axial position *trans* to the cysteine residue. Upon reduction of the iron ion (rubredoxin is the proposed electron donor),[45] the glutamate residue (pK_a= 4.25) no longer acts as the sixth ligand and moves away from the active site. The superoxide molecule (pK_a= 4.69) then binds to the ferrous ion in an end-on fashion speculated to be guided by a positively charged nearby lysine residue.[44] This lysine residue (pK_a= 10.5) protonates the superoxide to form a Fe^{3+}-hydroperoxo (Fe-OOH) species.[27, 46] This species, termed the "600-nm" intermediate giving rise to an absorption band at 600 nm in the electronic absorption spectrum, is formed at a nearly diffusion-controlled rate of $1.5\times10^{9}\,M^{-1}s^{-1}$.[27, 47, 48] In the final step, solvent protons are donated to the proximal oxygen of the Fe-OOH intermediate and a lysine residue to form hydrogen peroxide via Fe-O bond cleavage and regenerate the resting ferric form of the enzyme.[30]

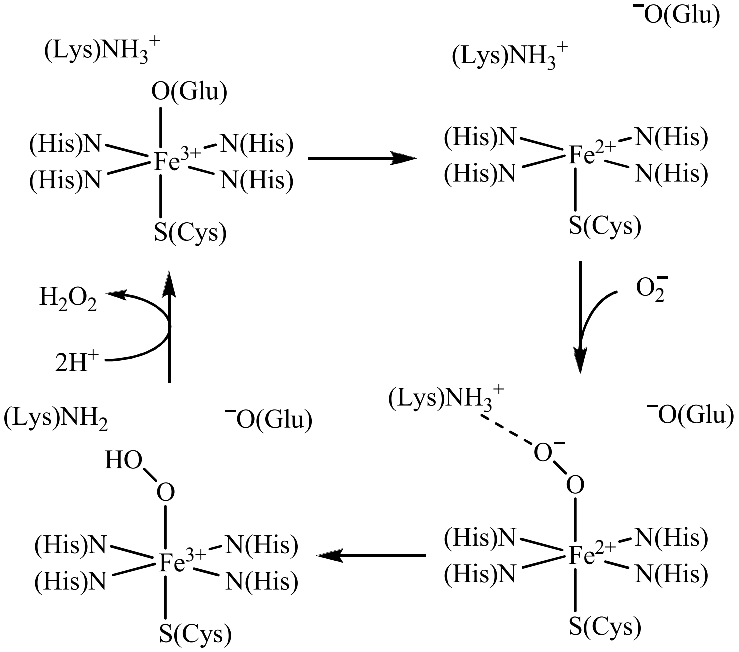

Scheme 1.1. The catalytic mechanism initiated by the non-heme iron enzyme SOR.[30]

The properties of the SOR enzyme are tuned such that the reduction of superoxide is achieved. Clay et al. have characterized the oxidized and reduced forms of SOR from *P. furiosus* using electron paramagnetic resonance (EPR), UV-visible spectroscopy, and variable-temperature magnetic circular dichroism (VTMCD).[49] An EPR redox titration was performed and the enzyme exhibited a one-electron redox potential at +250 ± 20 mV (versus NHE, pH 7.5). This is an optimum redox potential to catalyze the reduction of superoxide with the potential of the general reduction of $O_2^{\bullet-}$ to H_2O_2 being +890 mV (versus NHE).[50] According to the EPR spectrum, the iron center in SOR$_{ox}$ is high-spin ($S = 5/2$) in its ground state and remains high-spin upon coordination of superoxide analogue ligands such as azide (N_3^-). However, upon addition of cyanide (CN^-), the iron center transitions into a low-spin ($S = 1/2$) species. This transition results in the inhibition of the active enzyme and catalytic activity is diminished.

The UV-visible absorption spectrum as well as the VTMCD spectrum of SOR_{red} exhibits a transition at 320 nm (31,200 cm^{-1}) arising from the (His)N→ Fe^{2+} charge transfer (CT) transition as well as MCD bands centered at 295 nm (33,900 cm^{-1}) and 257 nm (38,900 cm^{-1}) arising from the (Cys)S→ Fe^{2+} CT transition.[49] In SOR_{ox}, the (Cys)S→ Fe^{3+} CT transition gives rise to a band at 660 nm (15,150 cm^{-1}). The SOR enzyme was found to be pH dependent, and the most stable at pH values between 5.0 and 9.5 determined by UV-visible spectroscopy.[51] Above pH 9.5, the absorption band arising from the (Cys)S^- → Fe^{3+} CT transition at 660 nm (15,150 cm^{-1}) undergoes a blue-shift to 588 nm (17,000 cm^{-1}) and is eventually lost upon increasing the pH.[49] Additionally, upon coordination of azide to SOR_{ox}, there is no significant effect on the absorption spectrum relative to the spectrum of the enzyme without an exogenous ligand; however, upon addition of cyanide, the (Cys)S^- → Fe^{3+} CT transition red-shifts to an energy of 685 nm (14,600 cm^{-1}) due to the high-spin to low-spin transition induced by the strong field ligand. The VTMCD spectra were also obtained for both forms of *P. furiosus* SOR.[49] The visible VTMCD bands assigned to the (Cys)S→ $Fe^{2+/3+}$ in the reduced and oxidized enzymes, respectively, exhibit a striking resemblance to one another. Each spectrum exhibits two different bands associated with the (Cys)S→ Fe transition, but the corresponding transitions are shifted to higher energy by approximately 15,500 cm^{-1} in SOR_{red}.[49]

The coordination reactions and electronic features of substrate analogues of SOR such as nitric oxide (NO) were also studied.[52] It was determined by EPR spectroscopy that an $\{Fe\text{-}NO\}^7$-type nitrosyl[53] formed upon reaction of NO with the SOR_{red} complex with a spin $S = 3/2$ species formulated through coupling of a high-spin Fe^{3+} ($S = 5/2$) antiferromagnetically with NO^-

($S = 1$). The FTIR and resonance Raman (rR) spectrum of the {Fe-NO}^{7} complex exhibited a band at 1,728 cm^{-1} assigned to the $\nu_{N\text{-}O}$ stretching mode and confirmed with a shift of 32 cm^{-1} upon ^{15}NO isotope labeling; this $\nu_{N\text{-}O}$ is observed in previously reported {Fe-NO}^{7} complexes which contain similar geometries about the iron center.[54, 55]

Synthetic Analogs of Superoxide Reductase

In order to better understand the intrinsic properties of the iron center in SOR and obtain insight on its catalytic mechanism, synthetic analogs of the active site have been generated. In order to successfully model the active site of SOR, a molecule must meet several requirements: (i) a designed planar neutral N_4 ligand frame (preferably with imidazole-N donors) containing a tethered or exogenous axial thiolate ligand *trans* to a vacant coordination site (ii) the iron center should be high-spin in both the 2+ and 3+ oxidation state, (iii) the quasi-reversible electrochemical event should be solely metal-based (e.g. no redox associated with thiolate ligand) and the Fe$^{2+/3+}$ potential of the molecule should be near the reported SOR potential of 250 mV (NHE), (iv) will bind substrate analogues like N_3^-, CN^-, or NO to form an {Fe-NO}^{7} species and (v) ideally coordinate and reduce superoxide in a proton-dependent fashion to generate the 600 nm intermediate and eventually H_2O_2 product at a catalytic rate.

A very common system utilized in the synthesis of SOR synthetic molecules is the cyclam ligand and derivatives thereof. The commercial availability and lack of oxygen sensitivity make this system a viable option for modeling the tetradentate netural N-donor plane of SOR. Halfen and coworkers synthesized an SOR analog utilizing a cyclam-containing system with tertiary amines, namely Me$_4$cyclam (Figure 1.2a).[56] The SOR analog was synthesized via the reaction of the Me$_4$cyclam with the product of $FeCl_2$ with triflic acid and further reaction with an exogenous, aromatic sodium thiolate salt affording the compound [(Me$_4$cyclam)Fe(SC$_6$H$_4$-*p*-OMe)]OTf (**1**) as shown in Figure 1.2b.

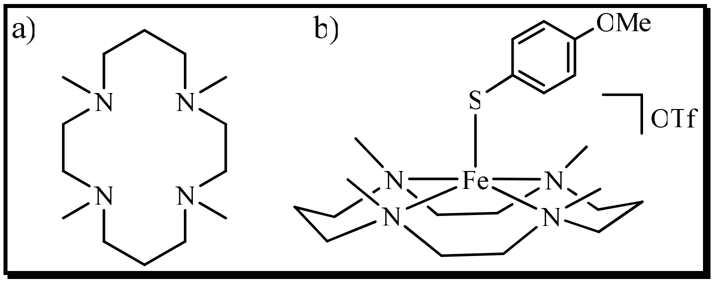

Figure 1.2. (a) The Me$_4$cyclam ligand. (b) [(Me$_4$cyclam)Fe(SC$_6$H$_4$-*p*-OMe)]OTf (**1**), a cyclam-containing SOR analog synthesized by Halfen and coworkers.[56]

The complex was determined to contain a high-spin Fe^{2+} (S = 2) ground state which is similar to SOR$_{red}$ and also contains a thiolate ligand *trans* to a vacant coordination site. However, the potential (+812 mV vs SHE, MeCN) of the compound proved to be irreversible and significantly more positive than the SOR value.[49] According to the X-ray analysis, compound **1** is also not purely square-pyramidal with a τ value[a] of 0.47 (τ = 0.0 for idealized sp and τ = 1.0 for idealized tbp).[56-58] The Fe-S bond in compound **1** (2.32 Å) is also shorter than the Fe-S(Cys) bond determined in the enzyme (2.40 Å) indicating the structural dissimilarities between compound **1** and the enzyme. While the structural characteristics do not model SOR exactly, the UV-visible properties of the S → Fe^{2+} CT transition of **1** are similar to SOR$_{red}$ with an absorption band occurring at 32,600 cm^{-1} (307 nm) (compared to the S → Fe^{2+} CT transition at 31,200 cm^{-1} (320 nm) in SOR). Compound **1** reacts with H$_2$O$_2$ to afford a high-valent Fe^{4+}=O moiety similar to what occurs at the active site of the heme-containing enzyme cytochrome P450.[59] However, the exogenous S-donor ligand in the axial position of the coordination sphere dissociates from the iron center in the Fe^{4+}=O species. The successful reactivity of **1** with

---

[a] $\tau = (\beta-\alpha)/60$ (τ = 0.0 for idealized sp and τ = 1.0 for idealized tbp)[58]

superoxide is more akin to P450 indicating an electronic perturbation in the model that is likely a reason for the lack of SOR activity.

Another analog synthesized by the same group is very similar to the previously described SOR model **1**. This compound contains a tethered thiolate donor to a cyclam ligand to complete the $[Fe(N_4)(S)]^+$ coordination sphere, which would presumably enhance the thermodynamic stability of the complex through the chelate effect. The researchers synthesized the compound with the reaction of the cyclam derivative with $[Fe(MeCN)_2(OTf)_2]$ and exchanging the counteranion with PF_6^- to afford $[LFe]PF_6$ (**2**), shown in Figure 1.3.[56]

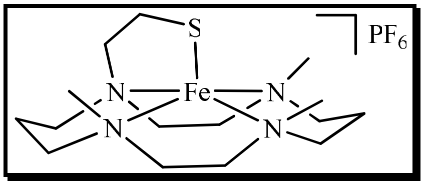

Figure 1.3. $[LFe]PF_6$ (**2**), an SOR analog synthesized by Halfen and coworkers containing a tethered thiolate ligand.[56]

Similarly to **1**, complex **2** contains a high-spin ($S = 2$) Fe^{2+} ground state similar to SOR_{red} according to magnetic susceptibility measurements as well as the respective Fe-N bond lengths (average Fe-N: 2.201 Å). The complex is also not purely square-pyramidal with a τ value of 0.5. The Fe-S bond in compound **2** (2.30 Å) is shorter than that found in the enzyme further indicating the structural impositions of the ligand frame that are absent in the enzyme. The electrochemical properties of compound **2** are also very similar to **1** and dissimilar to the SOR enzyme with an irreversible oxidation potential of +772 mV (vs SHE, MeCN). The absorption spectrum of **2** was also very similar to SOR_{red} giving rise to a transition at 30,450 cm^{-1} (328 nm) (compared to 31,200 cm^{-1} for SOR_{red}) for the $\pi \rightarrow \pi^*$ transition as well as a transition at 38,000 cm^{-1} (263 nm) (compared to 38,900 cm^{-1} (257 nm) for SOR_{red}) for the $\sigma \rightarrow \sigma^*$ transition.[56] This spectral similarity of exhibiting multiple S → Fe^{2+} transitions makes compound **2** a more similar SOR analog than **1**. Compound **2** also reacted with H_2O_2 to afford a high-valent Fe^{4+}=O species, but unlike compound **1**, the appended thiolate ligand remained in the coordination sphere of the complex as evidenced by the Mössbauer spectrum containing a smaller ΔE_Q than the spectrum resulting from compound **1**.[59] Again, this species models the cytochrome P450 enzyme more closely than SOR due to formation of the low-spin Fe^{4+}=O species when reacted with H_2O_2.

A third cyclam containing SOR model system has been synthesized by Kovacs and coworkers.[60, 61] Similar to the Halfen complexes, the cyclam contains a tertiary amine tethered with a thiolate ligand but slightly differs with three secondary amine nitrogen donors (Figure 1.4). This compound was synthesized anaerobically via the reaction of $FeCl_2$ with cyclam-PrS-Ac·4HCl affording the complex [Fe(cyclam-PrS)](BPh_4) (**3**).

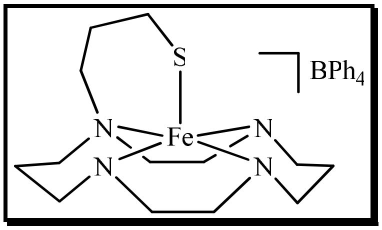

Figure 1.4. [Fe(cyclam-PrS)](BPh_4) (**3**), a cyclam SOR analog containing secondary amines and an appended thiolate synthesized by Kovacs and coworkers.[61]

Compound **3** shows a more square-pyramidal geometry than the previously discussed cyclam systems with a τ value of 0.13 similar to SOR_{red}.[61] This complex is high spin Fe^{2+} ($S = 2$) according to magnetic susceptibility measurements. However, the Fe-S bond length of compound **3** (2.29 Å) is shorter than the enzyme (2.40 Å). The reactivity of compound **3** has been studied with superoxide, and it has been shown to form a metastable Fe-hydroperoxo intermediate upon the addition of a proton donor (MeOH). The Fe-O stretch at 419 cm^{-1} in the resonance Raman (rR) spectrum of the intermediate formed via the reaction of **3** and superoxide (18-crown-6-K^+ salt) is lower in energy than previously reported iron peroxides[62] but similar to that of the enzyme (438 cm^{-1}).[27] Additionally, the O-O stretch at 891 cm^{-1} is higher than the reported range (820-860 cm^{-1})[62] indicating that the release of hydrogen peroxide is highly favored over O-O bond cleavage observed in the previously discussed cyclam systems. Upon the addition of acetic acid as a proton donor, the complex releases hydrogen peroxide as monitored by an amplex red assay and the formation of $[Fe^{3+}(cyclam\text{-}PrS)(OAc)]^+$ occurs modeling the glutamate-bound SOR_{ox}. Compound **3** shows an electrochemical event at $E_{1/2}$ = +220 (vs SCE, DMF) that is very similar to the enzyme value. To date, **3** is the only known functional SOR model.

Goldberg and coworkers have also utilized a cyclam derivative, namely 1,4,8,12-tetraazacyclopentadecane that contains four secondary amines (Figure 1.5). Additionally, a thiolate donor is added exogenously and was varied in order to probe the electronic properties upon variation of the axial S-donor.[63] The complex was formed via the reaction of $[Fe(H_2O)](BF_4)_2$ with the tetraamine donor ($[15]aneN_4$) followed by the addition of the sodium thiolate to afford the complex of $[Fe([15]aneN_4)(SR)]BF_4$ (**4**) (where R = aromatic entity) (Figure 1.5).

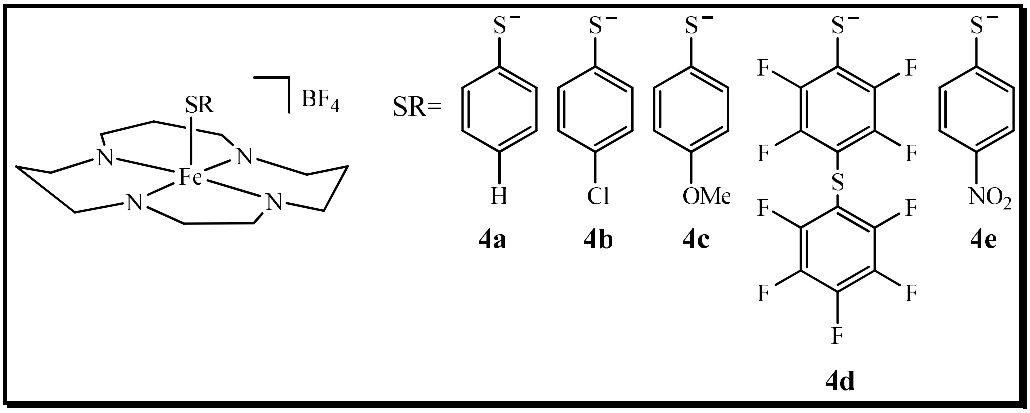

Figure 1.5. $[Fe([15]aneN_4)(SR)]BF_4$ (**4**), a derivative of the cyclam system varying the thiolate ligand produced by Goldberg and coworkers.[64]

While all of the compounds exhibit a five-coordinate Fe^{2+} complex with one vacant coordination site *trans* to the thiolate ligand, the most square-pyramidal coordination geometry contained the *p*-NO_2 thiolate ligand (**4e**) (τ value of 0.27) while the remaining complexes (**4a-4d**) have a τ value of approximately 0.5. Additionally, the Fe-S bond distances are shorter in **4** (range: 2.32-2.34 Å) than the Fe-S bond distance exhibited in the enzyme. The electrochemical properties of compound **4** were investigated resulting in irreversible oxidation events that differ depending on the nature of the para substituent on the aromatic thiolate. As expected the general trend is an increase in the oxidation potential as the thiolate ligand is varied from more electron-donating to electron-withdrawing.[63] However, all of these compounds contain a higher potential than the enzyme ranging from 651 mV to 1018 mV (vs Ag/AgCl, CH_2Cl_2). Compounds **4a-4e** were reacted with alkylhydroperoxides (^{t}BuOOH and cumenylOOH), and the absorption spectrum of the resulting low-spin complexes was obtained.[63] The spectrum of each alkyl-peroxo complex exhibited a band ranging from 508 to 526 nm higher in energy than the proposed 600 nm Fe-hydroperoxo intermediate present in the enzyme.[65] While the Fe-O bond is weaker (600-650 cm^{-1}) than those previously reported for the low-spin Fe^{3+}-OOR species,[66] the researchers also determined the Fe-O bond strength to be highly affected by the identity of the thiolate with an increase in the stretching frequency of the Fe-O upon increasing the electron-withdrawing capability of the thiolate ligand. It was also determined that the O-O stretching frequency (approximately 800 cm^{-1}) was not affected by the thiolate donor and was comparable to that of previously reported O-O bond lengths in low-spin Fe^{3+}-OOR species.[66] Compound **4** confirms the low-spin Fe-OOH species is supported in a FeN_4S coordination sphere. Because the spin state of the intermediates are not similar to that found for SOR, it is difficult to treat compound **4** as a direct functional analog of the enzyme; therefore, the SOR ligand is preventing the iron center from becoming low-spin during the catalytic cycle. This system does, however, provide evidence for the strong effect of the thiolate donor on the Fe^{3+}/Fe^{2+} potential of the iron center required to selectively reduce superoxide to hydrogen peroxide.

There is another class of SOR synthetic models that does not contain the cyclam entity. Halfen and coworkers have devised one such model with a tetradentate neutral nitrogenous system containing two pyridine moieties.[41] These aromatic ligands are more similar to the imidazole ligands of SOR_{red} than the previously discussed cyclam systems. The pyridyl-appended diazacyclooctance ligand, L^8py_2, was combined with $[Fe(H_2O)_6](BF_4)_2$ to form the Fe-N_4 entity which is further reacted with an aromatic sodium thiolate salt in MeOH to form the square-pyramidal complex $[L^8py_2Fe(SR)]^+$ (**5**) as shown in Figure 1.6. Compound **5** contains a thiolate ligand *trans* to a vacant coordination site in predominantly square-pyramidal geometry ($\tau = 0.15$).[56] Unlike most of the cyclam systems (**1-4**), compound **5** is more structurally similar to the active site of SOR_{red} but electronically different. The proposed CT transition is blue-shifted 9,000 cm^{-1} (approximately 250 nm) relative to the enzyme.[33] Additionally, the Fe-S bond present in **5** was determined to be 2.259 Å which is shorter than the reported Fe-S(Cys) bond distance of SOR_{red}. The potential of the Fe^{2+}/Fe^{3+} couple for compound **5** was determined to be irreversible at +857 mV (vs SHE, MeCN) which, like the previous systems, is too positive to catalytically reduce superoxide.[40] The reaction of **5** with ^{t}BuOOH in CH_2Cl_2 afforded high-spin alkylperoxo-Fe^{3+} intermediates as evidenced by absorption spectroscopy and exhibited $\nu_{Fe\text{-}O}$ and $\nu_{O\text{-}O}$ bands at 624 cm^{-1} and 832 cm^{-1} in the resonance Raman spectrum, resepectively.[67]

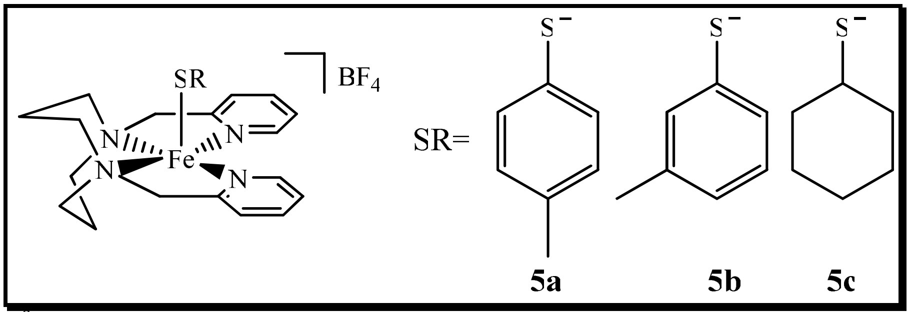

Figure 1.6. [L^{8}py$_2$Fe(SR)]$^+$ (**5**), pyridyl-appended SOR analog synthesized by Halfen and coworkers.[40]

Another non-cyclam SOR model was synthesized by Kovacs and coworkers with the designed N$_4$S-pentadentate ligand resulting in a trigonal bipyramidal Fe^{2+} complex.[68, 69] However, this compound contains a thiolate ligand *cis* to an available coordination site which is not observed in the enzyme and with previously discussed SOR models. The compound was synthesized via the reaction of 3-mercapto-3-methyl-2-butanone and tris(2-aminothyl)amine with FeCl$_2$ affording the compound [Fe(S^{Me2}N$_4$(tren))]PF$_6$ (**6**) (Figure 1.7). The trigonal bipyramidal complex consists of a low-spin Fe^{3+} species which is unlike the enzyme. Despite the structural dissimilarity to the enzyme, **6** appears to reduce superoxide to hydrogen peroxide through a transient hydroperoxo intermediate.[70] The electronic absorption spectrum exhibits a transition arising from the presence of a proposed Fe^{3+}-hydroperoxo intermediate at 582 nm in MeCN. This spectrum is similar to the proposed hydroperoxo intermediate observed at 600 nm for the enzyme.[65] The reported Fe-S bond length in **6** is 2.14 Å, though the role of the thiolate ligand *cis* to the vacant coordination site is unclear making the relative Fe-S bond distance irrelevant. Similar to compound **4**, the O-O bond stretching frequency for the low-spin Fe-hydroperoxo species derived from **6** is 784 cm^{-1}. This is weaker than the determined O-O bond of the intermediate on the catalytic cycle of SOR (850 cm^{-1}).[33] Extensive spectroscopic characterization of **6** as compared to SOR is not reported; therefore, it is difficult to establish compound **6** as an accurate analog of the active site of SOR due to its structural differences.

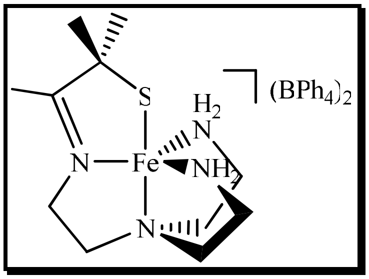

Figure 1.7. [Fe($S^{Me2}$$N_4$(tren))]$PF_6$ (**6**), a reported SOR analog with a thiolate *cis* to a vacant coordination site synthesized by Kovacs and coworkers.[68]

The synthetic analogs of the active site of SOR have brought about new insights into the mechanism by which SOR catalyzes the reduction of superoxide and their general properties are presented in Table 1.2. As has been determined through these modeling efforts, the role of the thiolate ligand *trans* to the vacant coordination apparently affects the strength of the Fe-O bond formed in the Fe-OOR (R = H or alkyl) intermediates. However, the length of the Fe-S bonds in the models presented is not comparable to the very long Fe-S bond in SOR (2.44 Å). This discrepancy could be due to the lack of hydrogen bonds to the thiolate ligand as found in the enzyme. In order to achieve optimum structural modeling of the active site, a model must successfully recreate the square-pyramidal coordination environment as well as the unusually long Fe-S bond length *trans* to the vacant coordination site, which appears to be crucial in the release of hydrogen peroxide from the iron center and also the high-spin nature of iron. Although several models employ cyclam-N_4 derived ligand frames, there appears to be drastic differences in terms of spin-state upon minor differences in this ligand and thus affords deviation in SOR chemistry. While the current synthetic analogs of the active site in SOR presented here have brought about important information regarding the properties of non-heme Fe/S systems, further research is required to shed more insight on the catalytic intermediates traversed along the reaction path and the overall mechanism of SOR. These findings could allow researchers to define and control properties that make iron perform specific and selective oxidation chemistry.

Table 1.2. The general properties of each SOR analog discussed.

Compound	Fe-N_{avg} (Å)	Fe-S_{avg} (Å)	Spin State	$E_{1/2}$ (mV) (vs. SHE)	O Int.[a]	Int. Spin State	O-O (cm^{-1})	Fe-O
1	2.221	2.322	hs	+812	Fe^{4+}=O	ls	NA	1.65 Å
2	2.201	2.297	hs	+772	Fe^{4+}=O	ls	NA	1.70 Å
3	2.171	2.286	hs	+464	Fe^{3+}-OOH	hs	891	419 cm^{-1}
4	2.170	2.330	ls	+651-+1018	Fe^{3+}-OO^{t}Bu	ls	801	614 cm^{-1}
5	2.206	2.291	hs	+857	Fe^{3+}-OO^{t}Bu	hs	832	624 cm^{-1}
6	2.152	2.329	ls	+21	$Fe^{3+}(\eta^1$-OOH)	ls	784	1.86 Å
[a] Note: the experimental setup with oxygen was inconsistent between compounds								

Intent of the Present Research

Our long-term goal is to further understand the role of iron in biology. The overall objective of this research, which is a step toward attainment of our long-term goal, is to determine the factors required to make iron a participant in biological redox reactions, specifically in the regulation of ROS. It is our central hypothesis that iron plays a role in the detoxification of reactive oxygen species in Fe-SOR because of the unique spatial disposition and electronic features of the N_4S coordination sphere promotes such reactions.

The research presented herein describes the synthesis and characterization of synthetic models of the active site of SOR containing a common neutral N_4 system where we add an exogenous thiolate ligand to complete the coordination sphere. The objective of such modeling studies is to understand the intrinsic properties that the ligands impart on the metal site in order to provide information on the catalytic mechanism at work in SOR. The utilization of neutral N_4 ligands (containing pyridine-N and for the first time imidazole-N donors) allows us to control the type of axial thiolate ligand we add to the corresponding Fe^{2+} precursor and provides strict and rigid planarity of the N-donors to prevent the formation of different Fe^{2+} coordination conformers. The effects of different substituents on the N_4 ligand and the different thiolate ligand and the unusual formation of eight-coordinate Fe complexes will be presented. It is expected that the systems described herein will provide a convenient and fast synthetic route towards five-coordinate Fe^{2+} complexes in an N_4S coordination sphere with one free axial position readily available to study the binding and reactivity of small molecules like superoxide and NO.

CHAPTER 2

SYNTHETIC MODEL CONTAINING PYRIDINE RINGS

Introduction

In the present study, we have synthesized and characterized models of the primary coordination sphere of the active site of SOR. In order to understand the effects of this basal place His_4 environment about the iron center, a planar non-macrocyclic N_4 nitrogenous ligand containing two pyridine rings and two imine-N nitrogens was employed as our ligand of choice. Although the histidine ligands of the enzyme contain imidazole-N donors, the pyridine ligands are utilized as the initial nitrogen donors due to the relative commercial availability of pyridine derivatives and the aromatic character of the pyridine ring compared with the imidazole ring. Pyridine rings have been utilized sparingly in previously reported SOR model systems,[40] and extensive studies on strictly planar ligand frames to impart a strictly square-pyramidal geometry about iron has not yet been employed.

Synthesis of Ligand (**L1**)

In this study, we chose to utilize the N_4 ligand 1,2-bis(2'-pyridylmethyleneimino)benzene (**L1**) as the nitrogenous donor set in our SOR model system. This ligand is predicted to closely mimic the properties of the four histidine ligands in the basal plane of the enzyme and should remain more rigid when coordinates than previously reported cyclam-derivitized models used in other SOR models.[56, 61, 63] Furthermore, the N_4 ligand is readily obtained in one step and allows for synthetic flexibility in the thiolate donor used at the one axial site. This affords an axial site *trans* to the thiolate that will be open or weakly bound to a coordinating solvent that should be available for reactivity studies. The synthesis of the pyridine-based ligand was performed via the Schiff base reaction of phenylene diamine and the corresponding carboxaldehyde. The synthesis of the ligand was attempted using previously reported methods in both MeOH and n-PrOH as reaction solvents; however, theses procedures failed to produce consistent results and the desired product was obtained in small yield (~15 %).[71-74] Therefore, a new procedure for the synthesis of **L1** was formulated in our laboratory taking advantage of the insolubility of the product in acetonitrile (MeCN) to afford the product in good yield (Scheme 2.1). Two molar equivalents of 2-pyridine-carboxaldehyde were added dropwise at room temperature (RT) to 1,2-phenylenediamine in MeCN and then allowed to reflux for 4 h. There was no notable change to the orange solution when heated. Upon cooling to RT, a pale yellow precipitate formed, which was collected and washed with cold MeCN. The yellow filtrate was concentrated via rotary evaporation and allowed to stir at RT. An additional batch of the pale yellow solid formed and was worked up in a similar manner. Yield: 40 %. ^{1}H NMR (298 K, $CDCl_3$, 400 MHz, ppm from TMS): 11.57 (s, 1H), 8.62 (d, 2H), 8.39 (d, 2H), 7.85 (t, 2H), 7.62 (s, 1H), 7.39 (t, 2H), 7.30-7.24 (m, 4H). Selected IR bands (diamond ATR, cm^{-1}) 1592 (w, $\nu_{C=N}$), 1439 (m), 1314 (m), 1278 (m), 740 (s), 701 (m). The characterization of L1 was consistent with previously reported data on this ligand.[72]

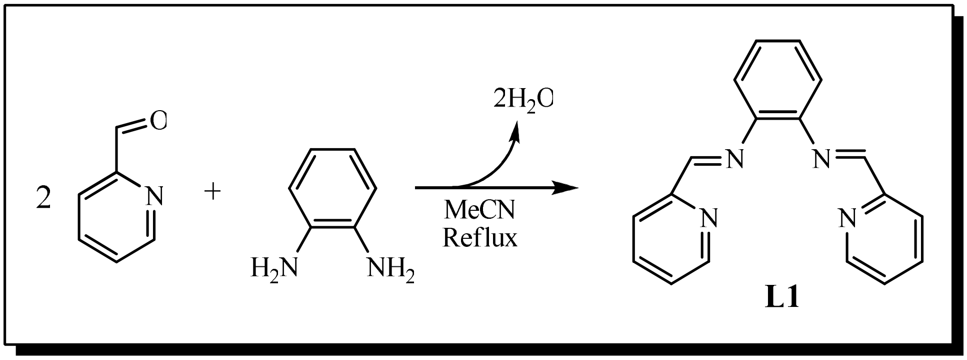

Scheme 2.1. Synthesis of N_4 ligand 1,2-bis(2'-pyridylmethyleneimino)benzene (**L1**).

The infrared spectrum of **L1** (Figure 2.1) displayed characteristic peaks that enabled characterization of the iron complexes. The absorption spectrum displayed a prominent π → π* transition at 308 nm (32,500 cm^{-1}, ε = 41,000 $M^{-1}cm^{-1}$) in the UV region with shoulders at 320 nm (31,250 cm^{-1}, ε = 31,000 $M^{-1}cm^{-1}$) and 239 nm (41,800 cm^{-1}, ε = 17,200 $M^{-1}cm^{-1}$) (Figure 2.2).

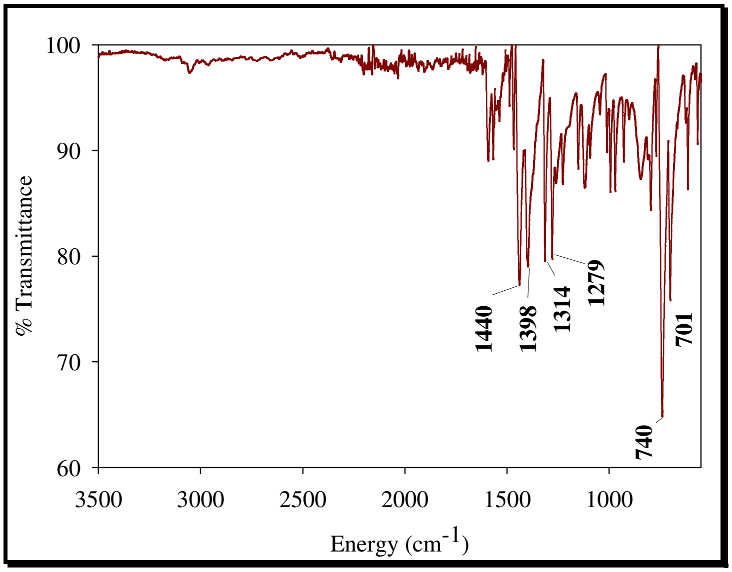

Figure 2.1. The infrared spectrum of **L1** with the characteristic peaks labeled (cm^{-1}).

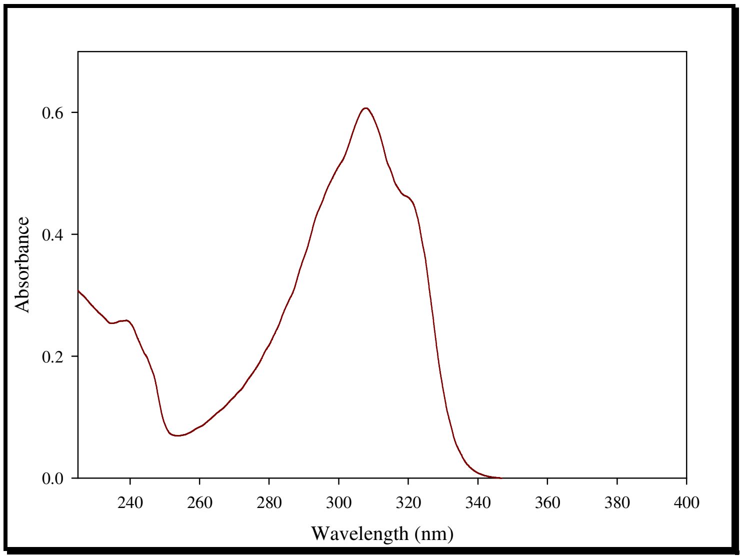

Figure 2.2. UV-visible absorption spectrum of **L1** in MeOH. λ = 308 nm (ε = 31,000 M^{-1} cm^{-1}) with shoulders at 320 nm and 240 nm resulting from a π → π* transition.

Preparation and Characterization of Fe Complexes

The first iron complexation reactions with **L1** was performed with the Fe^{III} precursor, $(Et_4N)[FeCl_4]$, in hopes of forming the $[Fe^{III}(L1)Cl_2]^+$ complex initially, which would then be followed by Cl displacement through thiolate addition to form $[Fe^{III}(L1)(SR)]^{2+}$ complexes. The Fe^{III} reactions served as our starting point due to the fact that this chemistry could be undertaken without the need for anaerobic conditions. The complex was synthesized by adding a methanolic (MeOH) solution of the Fe^{III} salt to an MeOH solution of **L1** to generate the red-colored $[Fe(L1)Cl_2]^+$ (**1**) complex. The electronic absorption spectrum in MeCN displayed a band at 308 nm (ε = 50,000 $M^{-1}cm^{-1}$) and a shoulder at 370 nm. To complete the coordination geometry observed in SOR, an MeOH solution of 4-chlorobenzenethiolate ($^{-}$SPh-*p*-Cl) (prepared from the addition of Na(s) to HSPh-*p*-Cl in MeOH) was added via cannula and stirred for 1 h resulting in a dark red/purple solution. The compound was precipitated with diethyl ether (Et_2O), and the proposed [Fe(L1)(SPh-*p*-Cl)(Cl)](Cl) complex (**2**) dark red solid was characterized via UV-vis and FT-IR.

Since the active form of SOR is in the Fe^{II} state we also prepared the corresponding Fe^{II} complexes. To achieve this result, we reacted an MeCN solution of **L1** with $[Fe(H_2O)_6](BF_4)_2$ to generate a pale red colored solution that we tentatively assign as $[Fe(L1)(MeCN)_2](BF_4)_2$ (**3**) as shown in scheme 2.2. Although the complex is proposed to be in an octahedral geometry, the identity of the substituents located in the axial positions has yet to be determined. The likely scenario is the presence of solvent in these positions due to the change in color from red to yellow when **3** stirred in Et_2O as a result of a slow exchange of the MeCN axial ligands for the bulk (Et_2O) solvent. Upon adding the $[Fe(L1)(Et_2O)_2](BF_4)_2$ solid to MeCN, the solution returns to its original red color.

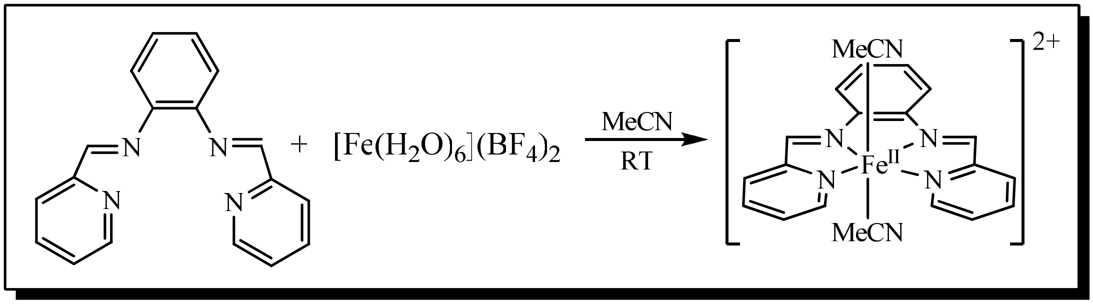

Scheme 2.2. Synthesis of the N_4-coordination complex $[Fe^{II}(L1)](BF_4)_2$ (**3**) with solvent in the axial positions.

The properties of compound **3** were analyzed with electrochemistry and FTIR spectroscopy. Electrochemical studies reveal a quasi-reversible feature at $E_{1/2} = 1.25$ V (vs Ag/AgCl, MeCN) (Figure 2.3) indicating some breakdown of the coordination sphere during oxidation to Fe^{III}. The FTIR spectrum of **3** displayed a prominent peak at 1049 cm^{-1} attributing to the BF_4^- counteranion in addition to the ligand peaks as shown in Figure 2.4.

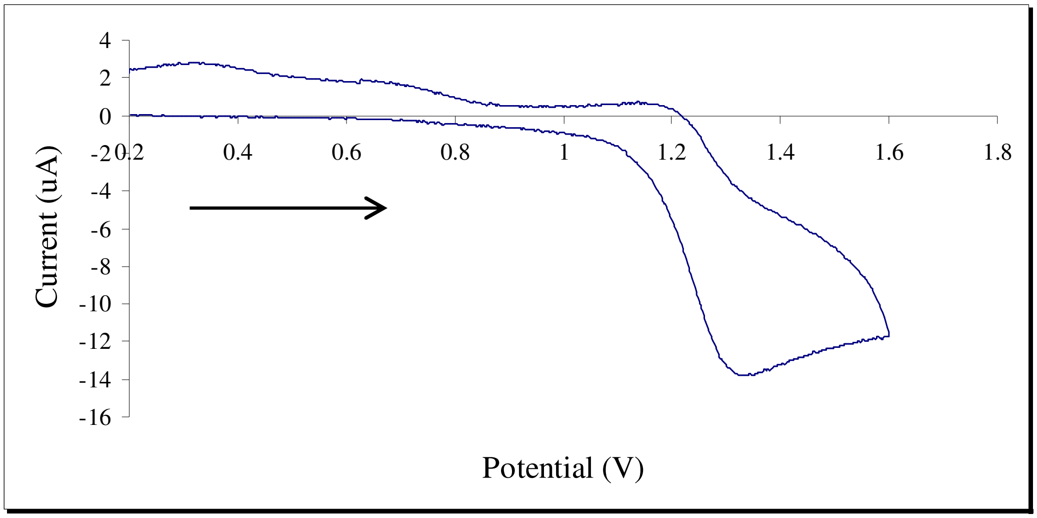

Figure 2.3. The cyclic voltammogram of $[Fe(L1)(MeCN)_2](BF_4)_2$ **3**. $E_{1/2} = 1.25$ V (vs Ag/AgCl in MeCN with 0.1 M $^tBu_4NPF_6$ supporting electrolyte, glassy carbon working electrode, Pt-wire auxiliary electrode, scan rate 50 mV/s, RT)

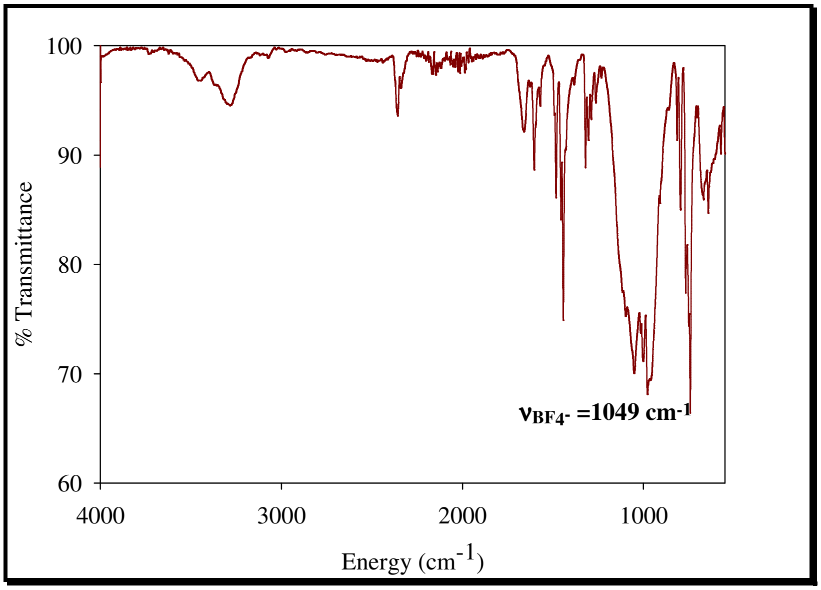

Figure 2.4. Solid state FT-IR spectrum of the compound [Fe(L1)]$(BF_4)_2$ (**3**) with a prominent peak at 1048.8 cm^{-1} arising from the BF_4^- counteranion (ATR).

To achieve FeN_4S-type complexes, we reacted thiolate donors with **3** in order to closely resemble the coordination of SOR. In order to achieve the FeN_4S SOR models, two different thiolate ligands were employed in this study: $^-$SPh-*p*-Cl and $^-SCPh_3$ to afford the complexes [Fe(L1)(SPh-*p*-Cl)]$^+$ (**4**) and [Fe(L1)$(SCPh_3)^+$ (**5**), respectively. These particular thiolate ligands were chosen to probe the affects of the electronic nature of the sulfur donor (alkyl vs aryl) and because of the large steric bulk, which prevent formation of six-coordinate FeN_4S_2 complexes and autoredox reactions. The basicity of the NaSPh-*p*-Cl thiolate is less electron-donating than the alkyl-$NaSCPh_3$ thiolate due to the relative electron density occupied by the benzene ring. Similarly to previously reported complexes utilizing exogenous thiolate donors,[63] sodium thiolate salts were synthesized from the reaction of the corresponding thiol with sodium hydride in tetrahydrofuran (THF) producing hydrogen gas and NaSR. The product was then added as an MeCN slurry to **3** also in MeCN to generate a dark red/purple solution. Compounds **4** and **5** were formed with both $[Fe(H_2O)](BF_4)_2$ (**a**) and $[Fe(H_2O)](ClO_4)_2$ (**b**) as the original iron salt starting material in order to observe the effects of the counteranion on the complexes.

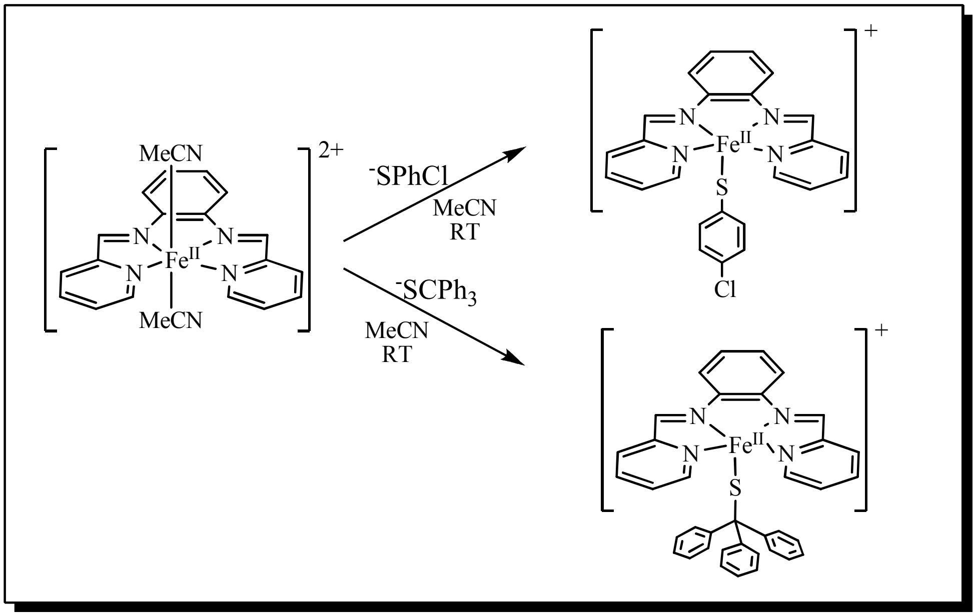

Scheme 2.3. Synthetic route to form the thiolate ligated SOR model complexes $[Fe(L1)(SPhCl)]^+$ (**4**) and $[Fe(L1)(SCPh_3)]^+$ (**5**).

The electrochemical properties of compound **4a** were studied (Figure 2.5). The cyclic voltammogram exhibited a broad feature at $E_{1/2}$ = 1.00 V (vs Ag/AgCl, MeCN). This feature is present in the cyclic voltammogram for the compound without a thiolate ligand in the axial position. This feature is most likely attributed to the Fe^{2+}/Fe^{3+} couple. The depression of the potential by 250 mV is due to the coordination of the thiolate ligand to the iron center.

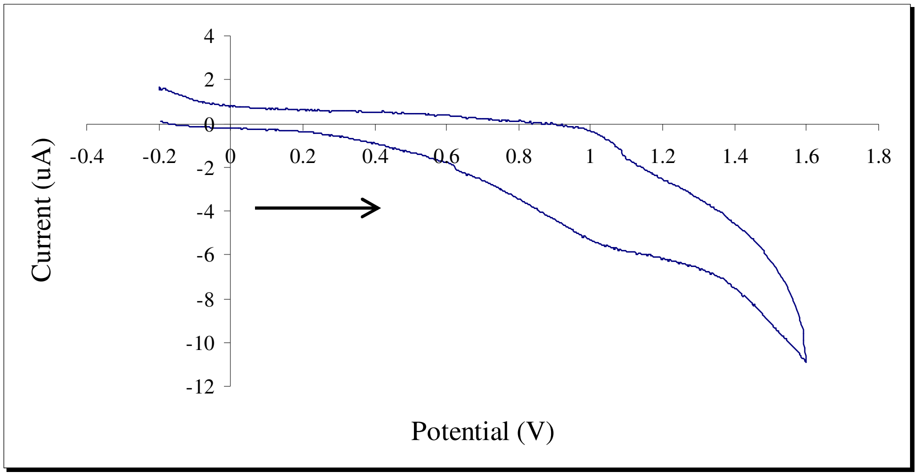

Figure 2.5. The cyclic voltammogram of compound **4a** with a neutral N_4 ligand. $E_{1/2}$ = 1.00 V (versus Ag/AgCl in MeCN with 0.1 M $^t\mathrm{Bu}_4\mathrm{NPF}_6$ supporting electrolyte, glassy carbon working electrode, Pt-wire auxiliary electrode, scan rate 50 mV/s, RT)

The FT-IR spectrum of compound **4a** shows the B-F stretch of the counteranion BF_4^- at ν = 1054 cm^{-1} as well as the bands corresponding to the ligand. The presence of one counteranion, as opposed to two as in compound **3**, is observable due to the relative intensities of the BF_4^- stretch which is more intense in the FT-IR spectrum of **3** (see Figure 2.4 and 2.6). The presence of the thiolate ligands is difficult to distinguish in the FT-IR spectrum. The bands associated with the two different thiolate ligands either coincide with the counteranion stretch or the ligand bands and are consequently "hidden" or are too weak to distinguish in the spectrum. Therefore, the FT-IR spectrum for compound **5** is very similar to that of compound **4**. The absorption spectrum of **4** in methanol displays a prominent band at 325 nm (30,700 cm^{-1}, ε = 40,000 $M^{-1}cm^{-1}$) most likely $\pi \rightarrow \pi^*$ in origin since the same transition is present in the absorption spectrum of **L1**. Additionally, the expanded region of the lower energy region reveals a band centered at 520 nm (19,200 cm^{-1}, ε = 1,350 $M^{-1}cm^{-1}$) that may be due to a d-to-d transition. Compound **4** was determined to be air-sensitive according to the electronic absorption spectrum after air exposure which exhibited a shift of the transition at 325 nm to 313 nm; additionally, the lower energy transition at 520 nm decreased in intensity.

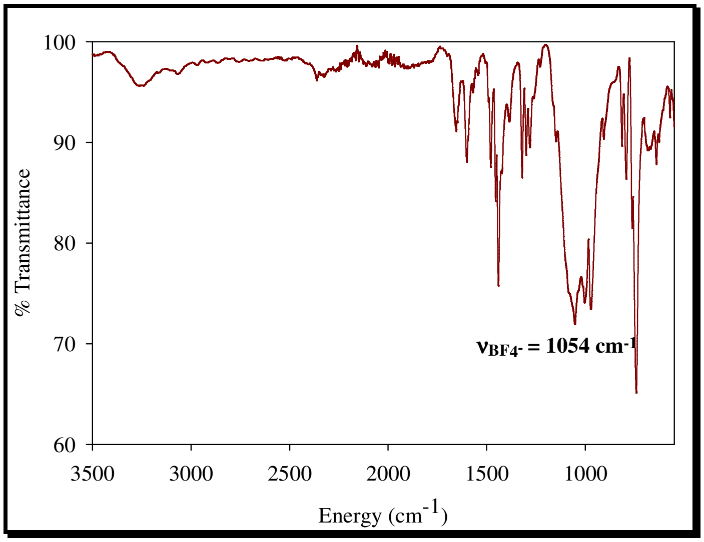

Figure 2.6. Solid state FT-IR spectrum of $[Fe(L1)(SPh\text{-}p\text{-}Cl)](BF_4)$ **4a** (ATR).

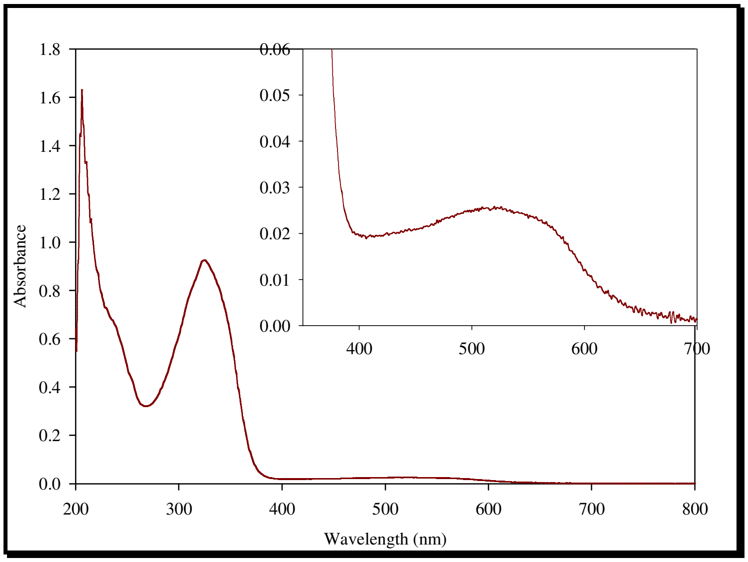

Figure 2.7. UV-vis spectrum of [Fe(L1)(SPhCl)](BF_4) **4** in MeOH (0.1 mM) at 298 K. *Inset:* The lower energy band at 520 nm (19,200 cm^{-1}, $\varepsilon = 1{,}350\ M^{-1}cm^{-1}$).

Reactivity of Fe Complexes

The ultimate goal of this study is to mimic the structure and ultimately the function of SOR via a synthetic analogue approach in order to understand the mechanism of superoxide reduction in the enzyme. In order to gain more insight on the mechanism of superoxide reduction, the reactivity of complexes **4** and **5** were probed with nitric oxide (NO). NO is a gaseous free-radical with many biological implications and is commonly used as a substrate analog of dioxygen derivatives like superoxide because of the structural similarity, radical character and non-innocent character of the diatom. The NO· donor utilized in this study, Ph_3CSNO, releases NO in the presence of transition metals and forms ½ mol equiv of trityl disulfide ($Ph_3CSSCPh_3$) as a benign byproduct that is readily separated from the Fe-NO complex. The reactivity of NO was probed with both complexes **4** and **5** (Scheme 2.4).

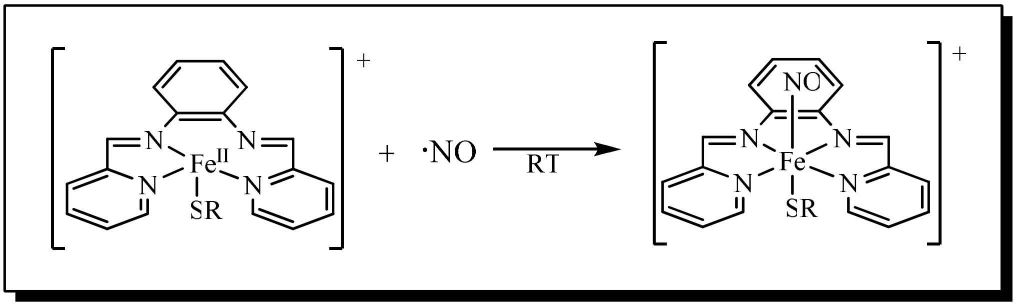

Scheme 2.4. General synthetic scheme for the formation of the Fe-NO complexes [Fe(L1)(SPhCl)(NO)](BF_4) (**6a**), [Fe(L1)(SPhCl)(NO)](ClO_4) (**6b**), [Fe(L1)($SCPh_3$)(NO)](BF_4) (**7a**), and [Fe(L1)($SCPh_3$)(NO)](ClO_4) (**7b**).

Upon reactivity with the NO donor, the $[Fe(L1)(SR)]^+$ compounds give rise to the presumably six-coordinate $[Fe(L1)(SR)(NO)]^+$ complexes that have been assigned as $\{Fe\text{-}NO\}^7$ type nitrosyls according to the Enemark-Feltham notation.[53] The absorption, FT-IR, and EPR spectra were obtained for each of the $\{Fe\text{-}NO\}^7$ products resulting from the reactivity of the model compound with NO. The complexes with BF_4^- counteranion (**6a** and **7a**) gave rise to an N-O stretch at ν_{NO}=1740 cm^{-1} as well as a prominent peak at ν_{BF4}=1053 cm^{-1} in addition to the signature **L1** bands (Figure 2.8). This band is strikingly similar to the FTIR ν_{NO} stretching mode observed in the enzyme at 1,728 cm^{-1}.[75] The 4.3 K X-band EPR spectrum of the $\{Fe\text{-}NO\}^7$ complex **6** reveals the presence of a complex giving rise to an S=3/2 species with g-values at 4.01, 3.79, and 2.01 (Figure 2.9).[75] This formulism results from a high-spin Fe^{III} center (S = 5/2) antiferromagnetically coupled to an NO^- ligand (S = 1). This is similar to previously reported inorganic $\{FeNO\}^7$ complexes which exhibit S = 3/2 systems.[54, 55, 76] Additionally, the resonance Raman data for these complexes also exhibit bands at 1712 cm^{-1} and 1776 cm^{-1} which were assigned as ν_{NO} stretching modes.[54, 55]

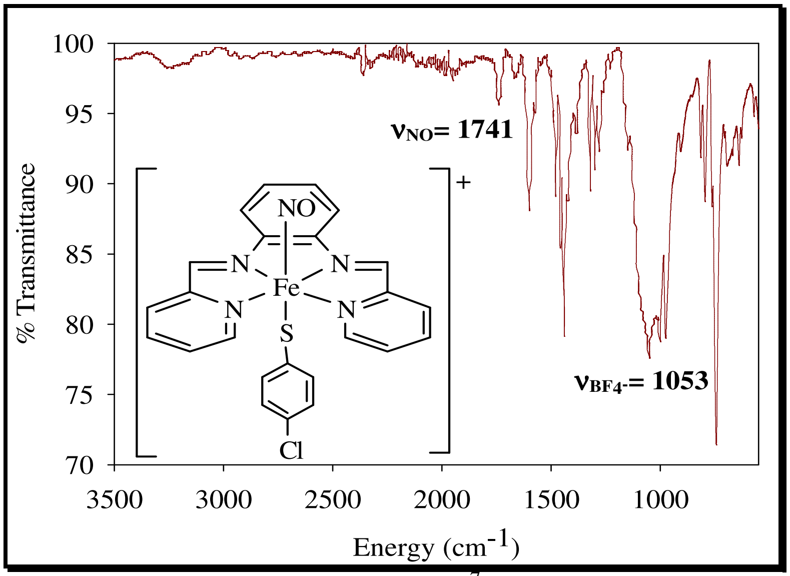

Figure 2.8. Solid-state FTIR spectrum of the $\{FeNO\}^7$ compound **6a** (ATR).

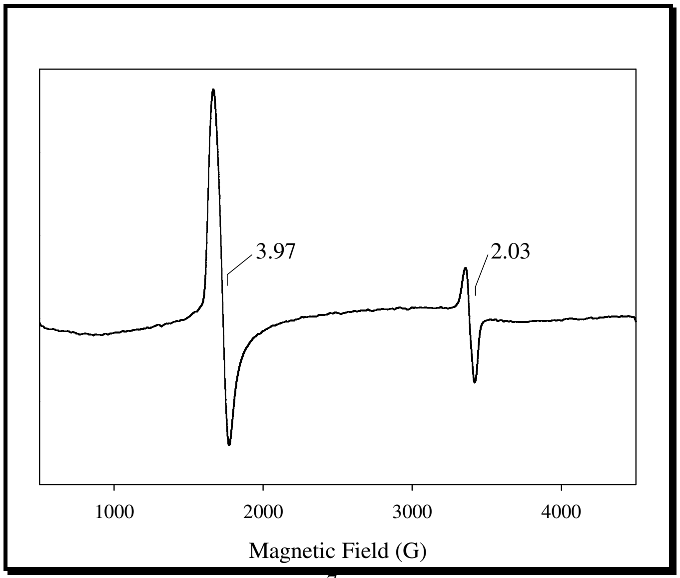

Figure 2.9. X-band EPR spectrum of $\{Fe\text{-}NO\}^7$ compound **6a** in toluene:MeCN (1:1) glass at 4.3 K. The spectrum was recorded at 9.60 GHz; modulation amplitude, 6.48 G; microwave power, 2.02 mW

The Mössbauer spectrum was also obtained for the $\{Fe\text{-}NO\}^7$ complex **6a** (Figure 2.10). This spectrum also exhibited a signal consistent with high-spin Fe^{3+} with an isomer shift (δ) of 0.48 mm/s.[77, 78] This supports the assignment of the EPR spectrum as an $S = 3/2$ signal. The electronic absorption spectrum of **6a** was analyzed upon exposure to air (Figure 2.11). The spectrum displayed a blue-shift in the energy of the transitions associated with the coordinated ligand from 329 nm to 307 nm upon exposure to air for 1 min. This peak also increased in intensity and is likely due to the oxidation of the Fe^{II} center to an Fe^{III} species ($\{FeNO\}^7$ to $\{FeNO\}^6$). Unlike the reactivity analyzed with cyanide and azide (*vide infra*), a peak appears at 239 nm arising from the Fe-NO compound which increases upon oxidation. The characterization of **6a** presented here indicates that NO is bound to the iron center analogous to the position at which it binds to the iron center in SOR. This suggests that **4a** is similar to the active site in SOR_{red}.

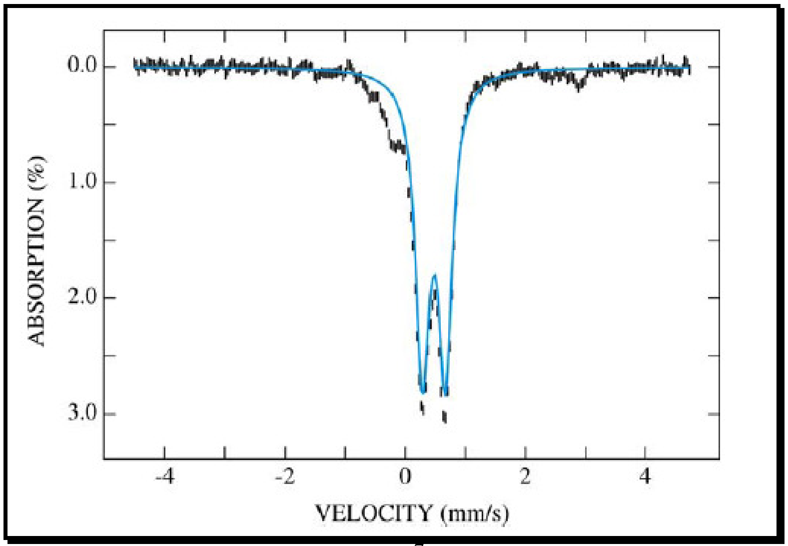

Figure 2.10. Mössbauer spectrum of the $\{Fe\text{-}NO\}^7$ complex **6a**. The spectrum was collected at 4.2 K in a weak magnetic field of 50 mT parallel to the γ-raditaion. The cyan line shown is the simulated spectrum of 85 % of Fe species with $\Delta E_Q = 0.38$ mm/s and $\delta = 0.48$ mm/s.

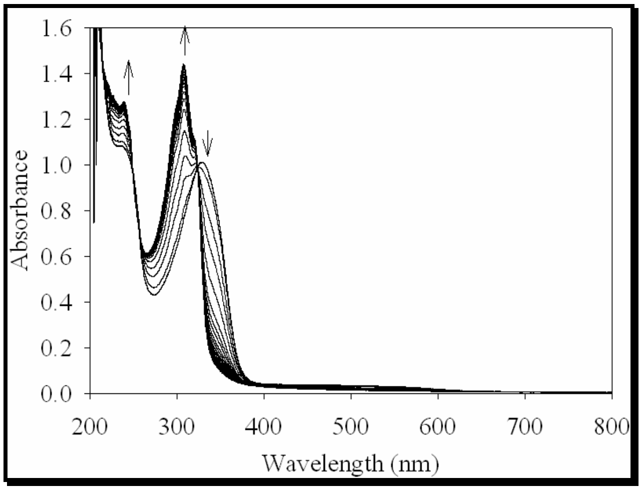

Figure 2.11. Changes in the electronic absorption spectrum of a 0.2 mM MeOH solution of {Fe-NO}^{7} compound **6a** exposed to air. The spectrum was recorded every 12 seconds at 298 K.

Similarly to **4a** and **5a**, the compounds utilizing ClO_4^- as the counteranion, compounds **4b** and **5b**, were also reacted with NO· to afford complexes **6b** and **7b**, respectively. The FTIR spectra of both complexes exhibited a band associated with the NO complexes at $\nu = 1740$ cm^{-1} in addition to the band arising from the ClO_4^- anion near 1100 cm^{-1} (Figure 2.12). The X-band EPR spectral analysis of **6b** and **7b** was recorded and is displayed in Figure 2.13. Complex **6b** gave rise to a low-spin Fe^{3+} rhombic species indicated in the X-band EPR spectrum at g = 2.47, 2.27, and 1.85. The rhombic signal is resultant of a low-spin Fe^{3+} species. An $S = 3/2$ species is also present in the sample indicated by the g-values 3.97 and 2.03. The spectrum indicates that there are multiple species present in the sample.

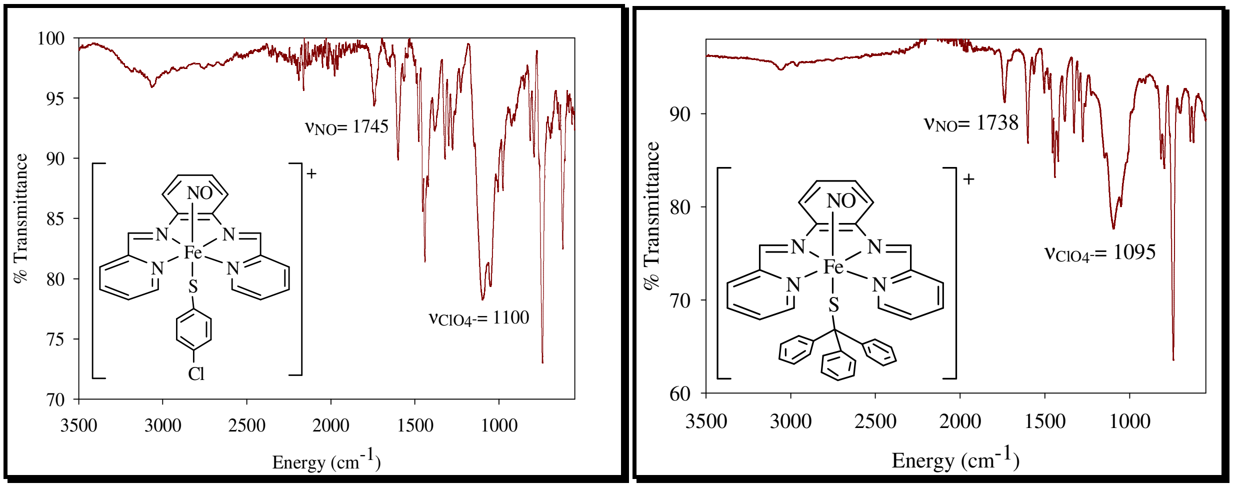

Figure 2.12. Solid-state FTIR spectra of **6b** and **7b** using ClO_4^- as the counteranion (ATR).

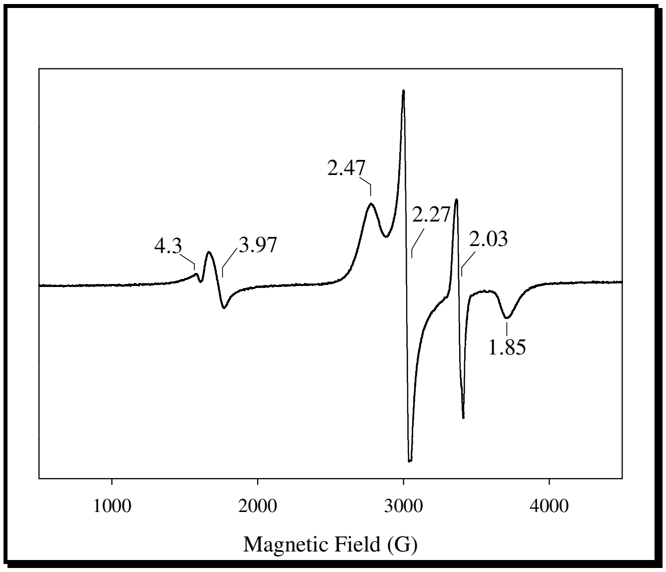

Figure 2.13. X-band EPR spectrum of **6b** in toluene:MeCN (1:1) glass recorded at 3.8 K. The spectrum was recorded at 9.60 GHz; modulation amplitude of 6.48 G; microwave power of 2.0 mW.

The X-band EPR spectra shown in Figure 2.14 for complex **7b** also gave rise to a rhombic species (g = 2.46, 2.26, 1.85). However, the g value at 2.03 is significantly more prominent resulting in the increase in the gain in order to observe the full signal. Again, there is a mixture in the sample, one being a six-coordinate low-spin Fe^{3+} species with an absence of NO ($S = 1/2$) and the other (arising from the more intense signal) is possibly the displaced trityl thiolate radical. Since both complexes utilizing ClO_4^- as the counteranion gave rise to a rhombic species in the EPR spectrum, it is possible that the perchlorate is oxidizing the Fe center making a $[Fe^{3+}(L1)(SR)]^{2+}$ species with possibly solvent bound in the axial position *trans* to the thiolate ligand. It has been reported that the oxidation of metals is possible in the presence of a perchlorate anion.[79-81] The reported iron oxidation occurs in an N_4-porphyrin system; therefore, it is very possible that the perchlorate anion is oxidizing the iron center resulting in a rhombic species absent of coordinated NO. Other evidence has been collected that possibly indicates the oxidation of the Fe center. The variation of the counteranion appears to alter the properties of the complexes (i.e. solubility and color). Though the preliminary data suggests that the oxidation of the iron species is possible, it is a tentative analysis since the structure of the complexes have not been acquired.

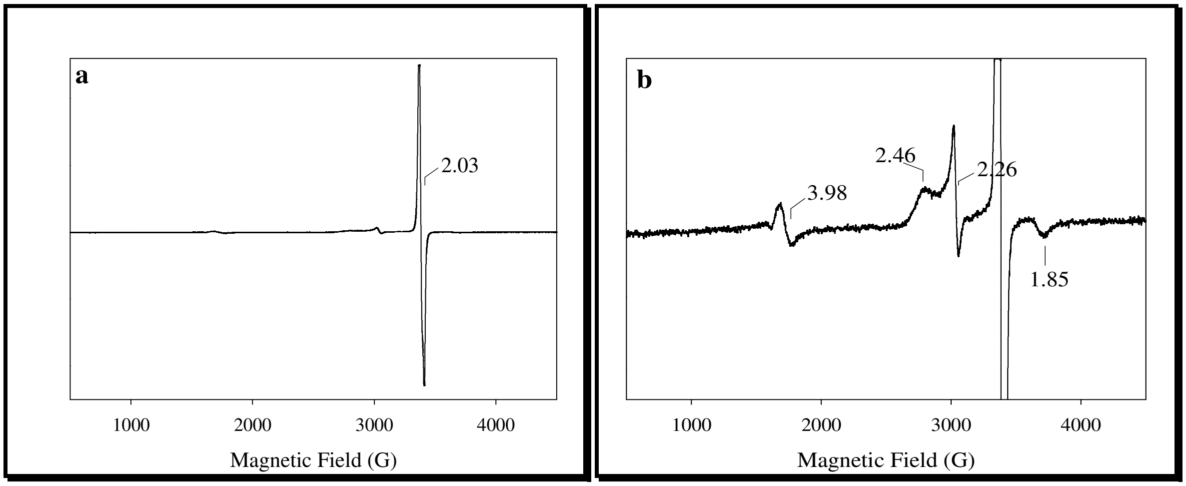

Figure 2.14. X-band EPR spectrum of **7b** in toluene:MeCN (1:1) glass at 3.8 K. (a) The receiver gain set at $1x10^4$ to fully view the g value at 2.03 (b) The receiver gain set at $2x10^5$ to amplify the rhombic signal at g = 2.47, 2.27, 1.85. The spectrum was recorded at 9.60 GHz; modulation amplitude, 6.48 G; microwave power, 2.0 mW.

The crystals resulting from the $[Fe(L1)(SR)(NO)]^+$ reactions were obtained after brief exposure to air and approximately one month of diffusing Et_2O into an MeCN solution affording dark red, rhombic crystals. The X-ray analysis for both compounds **6a** and **7a** were determined affording the six-coordinate product of the rearranged ligand $[Fe(L1')_3]^{2+}$ (**3a**) as shown in

Figure 2.15. The rearrangement of **L1** in the presence if ruthenium has been previously reported;[72] however, this is the first compound containing iron as the metal center in this complex. The result of the rearranged ligand in the determined structure is possibly due to the time in which the solutions unmoved. Upon exposure to air, the exogenous thiolate ligand must have been displaced resulting in the formation of disulfide, which has not been confirmed, and over time, the planar N_4 ligand rearranged resulting in the formation of **3a**.

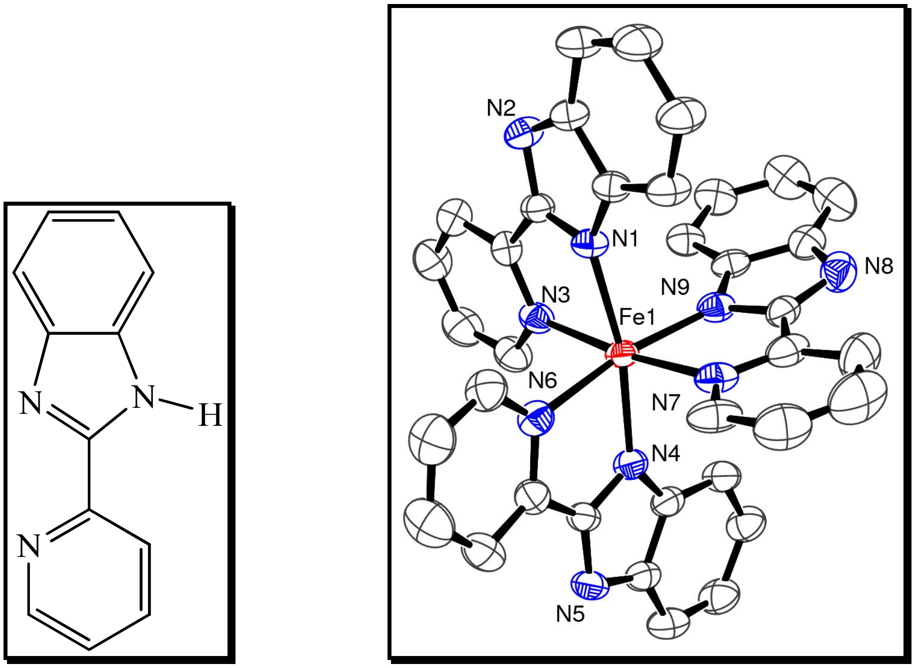

Figure 2.15. (Left) Schematic of rearranged **L1'.** (Right) ORTEP diagram of complex **3a** showing 30% thermal ellipsoids and atom numbering scheme for metal and heteroatoms.

Table 2.1. Summary of crystal data and intensity collection and structure refinement parameters for [Fe(L1')$_3$](ClO$_4$)$_2$•H$_2$O (**3a**•H$_2$O).

Parameters	**3a**•H$_2$O
Formula	$C_{36}H_{29}Cl_2FeN_9O_9$
Formula weight	858.43
Crystal system	Triclinic
Space group	*P*-1
Crystal color, habit	Red rectangle
a, Å	12.105(5)
b, Å	12.253(5)
c, Å	14.960(5)
α, deg	88.735(5)
β, deg	72.152(5)
γ, deg	73.108(5)
V, Å^3	2015.5(14)
Z	2
ρ_{calcd}, g/cm^{-3}	1.414
T, K	293(2)
abs coeff, μ (Mo Kα), mm^{-1}	0.570
θ limits, deg	2.13-28.26
total no. of data	27824
no. of unique data	9912
no. of parameters	514
GOF on F^2	1.022
R_1,[a] %	9.07
wR_2,[b] %	27.23
max, min peaks, e/Å^3	-0.450, 1.132

[a] $R_1 = \Sigma||F_o| - |F_c|| / \Sigma|F_o|$; [b] $wR_2 = \{\Sigma[w(F_o^2 - F_c^2)^2]/\Sigma[w(F_o^2)^2]\}^{1/2}$.

Table 2.2. Selected bond distances (Å) and bond angles (deg) for [Fe(L1')$_3$](ClO$_4$)$_2$•H$_2$O (**3a**•H$_2$O).

Fe(1)-N(1)	2.092(4)	N(1)-Fe(1)-N(9)	91.51(17)
Fe(1)-N(3)	2.139(5)	N(3)-Fe(1)-N(4)	94.85(17)
Fe(1)-N(4)	2.090(4)	N(3)-Fe(1)-N(6)	91.82(18)
Fe(1)-N(6)	2.142(5)	N(3)-Fe(1)-N(7)	173.25(16)
Fe(1)-N(7)	2.154(5)	N(3)-Fe(1)-N(9)	98.38(18)
Fe(1)-N(9)	2.067(5)	N(4)-Fe(1)-N(6)	77.66(18)
N(1)-Fe(1)-N(3)	78.15(17)	N(4)-Fe(1)-N(7)	91.61(17)
N(1)-Fe(1)-N(4)	169.02(18)	N(4)-Fe(1)-N(9)	97.93(18)
N(1)-Fe(1)-N(5)	158.14(8)	N(6)-Fe(1)-N(7)	91.4(2)
N(1)-Fe(1)-N(6)	93.97(18)	N(6)-Fe(1)-N(9)	169.22(18)
N(1)-Fe(1)-N(7)	95.74(17)	N(7)-Fe(1)-N(9)	78.8(2)
Fe(1)-N(1)	2.092(4)	N(1)-Fe(1)-N(9)	91.51(17)

Since both cyanide and azide are known to bind to the active site of SOR, and cyanide is a known inhibitor,[49] we probed the reactivity of these two small molecules with compound **4**. Both molecules are proposed to bind in the axial coordination site *trans* to the thiolate ligand affording the neutral compounds [Fe^{II}(L1)(SPh-*p*-Cl)(CN)] (**8**) and [Fe^{II}(L1)(SPh-*p*-Cl)(N_3)] (**9**) as shown in Scheme 2.5.

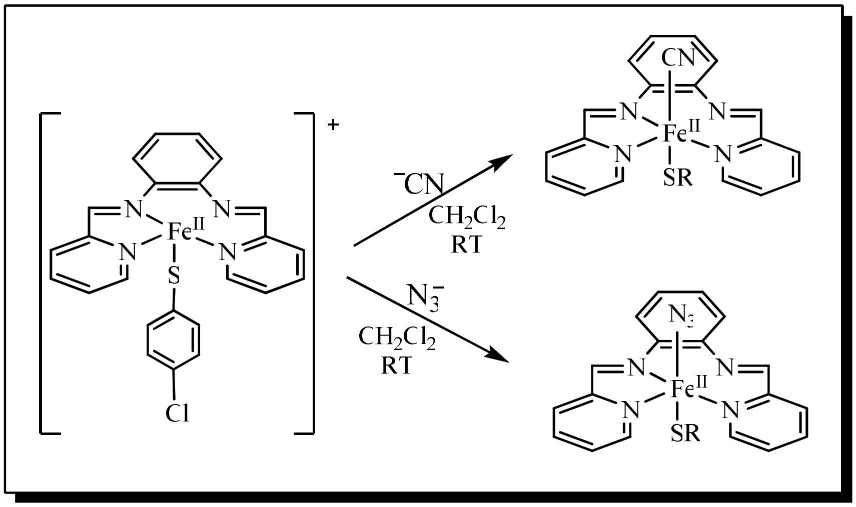

Scheme 2.5. Reactivity of model compounds with cyanide (top) and azide (bottom), which are both known to bind to the active site of SOR.

The reaction of the Fe^{2+} model compound **4** under anaerobic conditions with (Et_4N)(CN) resulted in a dark purple solid formulated to be the air-sensitive compound **6**. The FTIR spectrum of this solid exhibited one strong band at $\nu = 2074$ cm^{-1} supporting the formation of a linear mono-cyano species (Figure 2.17).[82] The O_2 sensitivity of this compound was revealed by monitoring its absorption spectrum upon exposure of a MeOH solution of the compound to air. The electronic absorption spectrum displayed a blue-shift of the high energy band associated with ligand $\pi \rightarrow \pi^*$ transitions from 322 nm to 308 nm as well as a red shift in the visible band from 550 nm to 556 nm similar to CN-bound SOR (Figure 2.16).[49] Confirmation of metal-centered Fe^{2+}-to-Fe^{3+} oxidation are from the corresponding X-band EPR spectrum of the chemically oxidized (with $FcPF_6$) complex run at 4 K that exhibits g-values near 2.0 consistent with low-spin Fe^{3+}, also similar to CN-bound SOR.[49]

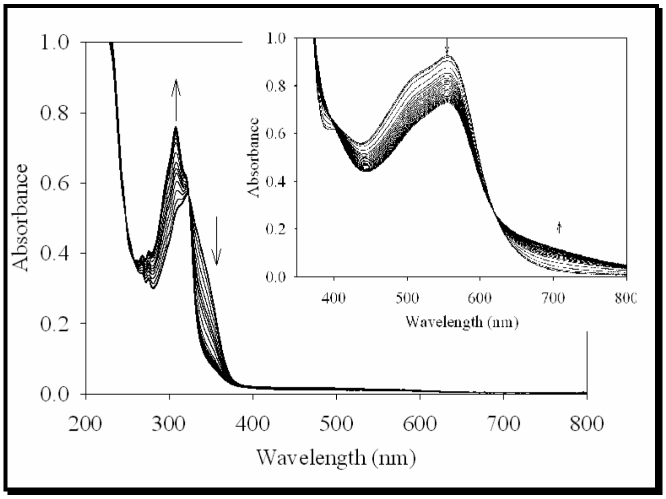

Figure 2.16. Changes in the electronic absorption spectrum of a 0.1 mM MeOH solution of compound **8** after exposure to air. Inset: Higher concentration (1.4 mM) experiment to show the changes in the visible transitions. Spectra were recorded every 12 seconds at 298 K.

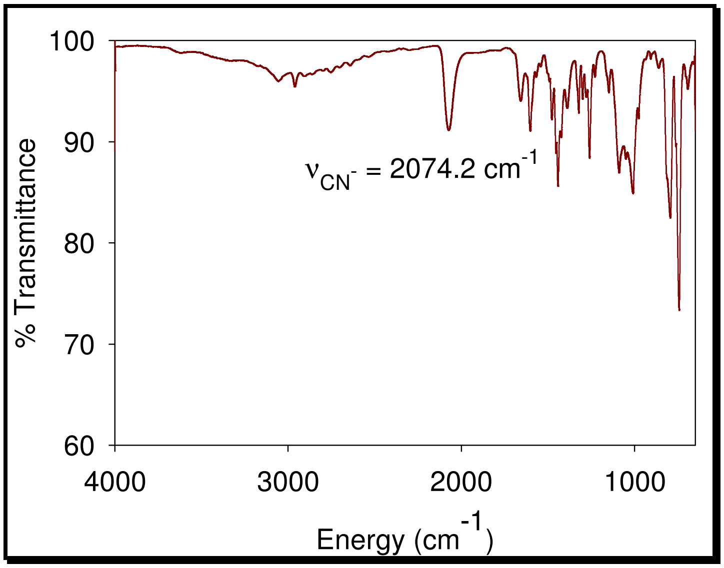

Figure 2.17. Solid-state FTIR spectrum of CN-bound SOR analog compound **8** (ATR).

Analogous to the reaction of [Fe(L1)(SPhCl)]$^+$ with CN$^-$, mixing one molar equivalent of (^{n}Bu$_4$N)(N$_3$) with compound **4** resulted in a light purple solid formulated as [Fe^{II}(L1)(SPhCl)(N$_3$)] (**9**). The corresponding FTIR spectrum of the azide species confirmed the formalism proposed above with one strong ν_{N3} peak at 2042 cm^{-1} (Figure 2.19).[83] Similar to the CN$^-$ compound, **9** also displayed air-sensitivity changing to a more red-colored compound after air exposure. The strong ν_{N3} peak in the FTIR spectrum shifted 5 cm^{-1} to 2047 cm^{-1} after exposure of the compound to air. Additionally, monitoring this change by UV-vis resulted in a blue-shift of the ligand charge transfer bands from 324 to 307 nm after the compound was exposed to air for approximately 1 minute (Figure 2.18). The visible transition at 495 nm also decreased in intensity and red-shifted to 580 nm. The isobestic points observed in the spectra also indicate a clean transition from the Fe^{2+} to the Fe^{3+} species with no observable intermediates.

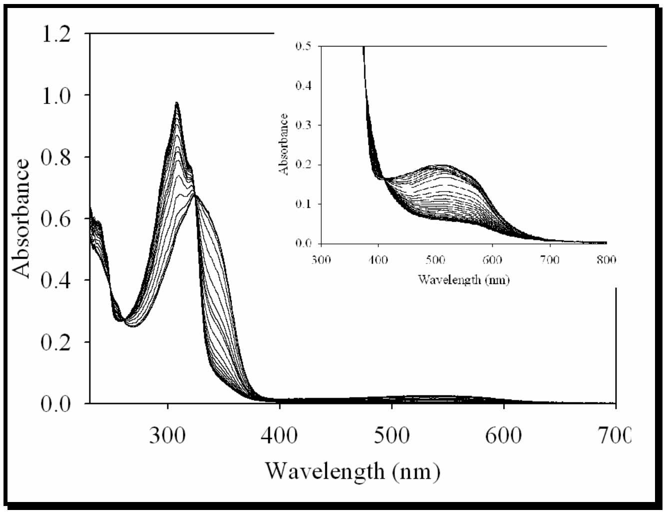

Figure 2.18. Changes in the electronic absorption spectrum of a 0.1 mM MeOH solution of compound **9** after exposure to air. An increase in absorption at 307 nm indicates the formation of an Fe^{3+} species. Inset: Higher concentration (0.8 mM) experiment to show the changes in the visible transitions. The spectra were recorded every 12 seconds at 298 K.

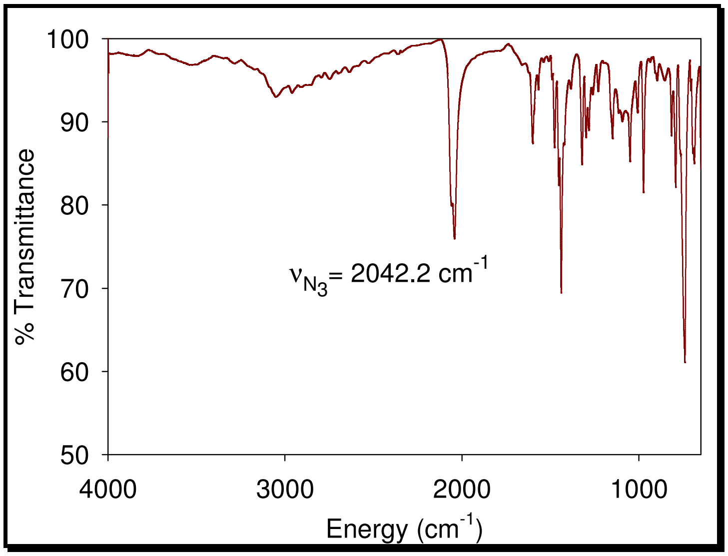

Figure 2.19. Solid-state FTIR spectrum of N_3-bound SOR analog compound **9** (ATR).

Conclusion

The neutral, pyridine-containing N_4 ligand presented here shows promising results for modeling the active site of SOR. The pyridine substituents of the ligand mimic the aromatic nitrogen donor ligands of SOR, and the exogenous thiolate ligand models the cysteine present in the enzyme. The reactivity of the FeN_4S compound was studied and resulted in similar reactivity to the enzyme consistent with an inner-sphere mechanism through direct electron transfer from Fe^{II} to superoxide. The presence of L1 with a thiolate ligand about an iron center exhibits a high-spin iron center analogous to that of SOR when reacted with nitric oxide. Additionally, both azide and cyanide bind to the iron center of the FeN_4S compound similarly to the enzyme. However, the compound of interest was not successfully crystallized affording a rearranged ligand bound to the iron ion upon crystallization after months of Et_2O diffusion.

Experimental Section

General Procedures. Manipulations for air- and moisture-sensitive materials were carried out under anaerobic an atmosphere of nitrogen using standard Schlenk techniques or in an MBraun glovebox under an atmosphere of purified nitrogen. All reagents were purchased from commercial suppliers and used as received unless otherwise noted. Diethyl ether, dichloromethane, and acetonitrile were purified by passage through activated alumina columns using an MBraun Solvent Purification System. Methanol was freshly distilled from $Mg(OMe)_2$ under N_2 prior to use. All solvents were stored over 3 Å molecular sieves in an anaerobic glovebox or under N_2 in a Schlenk flask prior to use. The nitrosothiol, Ph_3CSNO was synthesized following a published procedure. For reactions involving NO, care was taken to prevent light exposure by covering reaction glassware in aluminum foil or by performing experiments in a darkened room.

Physical Methods. Electronic absorption spectra were recorded on a Varian Cary 50 spectrophotometer at 25° C in air-tight Teflon-capped quartz cells. FTIR spectra were obtained using a Nicolet 6700 FT-IR from Thermo Fisher Scientific Inc., on a diamond ATR crystal running the OMNIC software. NMR spectra were recorded at on a Varian 300 MHz NMR spectrometer with chemical shifts referenced to TMS. Elemental analyses were performed by Quantitative Technologies Inc., Whitehouse, NJ. X-band EPR spectra were recorded on a Bruker ESP-300E EPR spectrometer (9.60 GHz) equipped with an Oxford Instruments ESR-9 flow cryostat. Spectra were recorded in 4 mm o.d. quartz EPR tubes capped with tight-fitting Teflon seals.

Synthesis of 1,2-bis(2'-pyridylmethyleneimino)benzene (L1). The synthesis of **L1** was attempted using previously reported methods in both MeOH and n-PrOH but herein we report a different procedure. To a solution of 1,2-phenylenediamine (1.0 g, 9.2 mmol) in MeCN (20 mL) was added a solution of 2-pyridine-carboxaldehyde (1.99 g, 18.6 mmol) in MeCN (5 mL) dropwise at room temperature and then refluxed for 4-5 hours with no notable changes. Upon cooling to room temperature (RT), a pale yellow solid formed. This solid was filtered off and washed with cold MeCN. The yellow filtrate was concentrated via a rotary evaporation and allowed to stir at RT. Additional pale yellow solid formed and was collected via filtration and washed with cold MeCN. Again, the filtrate was collected and concentrated resulting in more pale yellow solid. Yield: 0.6833 g (30.7%). ^{1}H NMR (298 K, $CDCl_3$, 400 MHz, ppm from TMS): 11.57 (s, 1H), 8.62 (d, 2H), 8.39 (d, 2H), 7.85 (t, 2H), 7.62 (s, 1H), 7.39 (t, 2H), 7.30-7.24 (m, 4H). Selected IR bands (diamond ATR, cm^{-1}) 1592 (w, $\nu_{C=N}$), 1439 (m), 1314 (m), 1278 (m), 740 (s), 701 (m). The characterization of L1 was consistent with previously reported data on this ligand.[72]

Synthesis of [Fe^{III}(L1)(Cl$_2$)]Cl (1). To a solution of L1 (104.6 mg, 0.36 mmol) in dry MeOH (15 mL) was added a solution of [Et$_4$N][FeCl$_4$] (118.6 mg, 0.36 mmol) in MeOH (10 mL) and stirred. The MeOH was removed and CH_2Cl_2 was added to precipitate Et$_4$NCl and filtered. The resulting solution was set up for crystallization by diffusion of Et_2O into an MeCN solution of the complex, but no distinguishable crystals resulted. Selected IR bands (diamond ATR, cm^{-1}): 1603 (w, $\nu_{C=N}$). Electronic absorption spectrum in MeCN, λ_{max} nm (ε, M^{-1} cm^{-1}) : 308 (~50,000), 370 (sh).

Synthesis of [Fe^{III}(L1)(SPhCl)]Cl$_2$ (2). To a solution of [Fe^{III}(L1)(Cl$_2$)]Cl(0.0996 g, 0.22 mmol) in MeOH (15 mL) was added a methanolic solution of NaSC$_6$H$_4$-*p*-Cl (0.0297 g, 0.21 mmol) (prepared from the addition of 1.2 mol eq of Na to 4-chlorobenzenthiol in methanol) via cannula and stirred for one hour resulting in a dark red solution. The compound was precipitated with Et_2O.

Synthesis of [Fe^{II}(L1)(SPh-*p*-Cl)]BF$_4$ (4a). This procedure was completed in the same manner as SOR models previously reported. The following procedure is a variation: To a solution of Fe(BF$_4$)$_2$·6H$_2$O (58.6 mg, 0.17 mmol) in MeCN (3 mL) was added a solution of L1 (50.0 mg, 0.17 mmol) in MeCN (4 mL) and stirred. This addition resulted in a red homogenous solution. To this solution was added a solution of NaSC$_6$H$_4$-*p*-Cl in MeCN (prepared from the addition of NaH to HSC$_6$H$_4$-*p*-Cl in THF) and allowed to stir resulting in a dark red solution. The solution was concentrated, and CH_2Cl_2 was added to precipitate the NaBF$_4$ salt. The solution was filtered through Celite yielding a dark red filtrate. The compound was precipitated and the red solid was isolated. This synthesis was also completed through forming the tetraethylammonium thiolate salt added to the Fe^{II} solution resulting in the precipitation of $(NEt_4)(BF_4)$ with addition of CH_2Cl_2. Selected IR bands (diamond ATR, cm^{-1}): 1603 (w, $\nu_{C=N}$), 738 (m, ν_{SC}). Electronic absorption spectrum in MeCN, λ_{max} nm (ε, M^{-1} cm^{-1}) : 309 (~50,000).

Synthesis of [Fe^{II}(L1)(SPh-*p*-Cl)]ClO$_4$ (4b). This procedure was completed in the same manner as SOR models previously reported. The following procedure is a variation. To a solution of $Fe(ClO_4)\cdot 6H_2O$ (42.0 mg, 0.165 mmol) in MeCN (5 mL) was added a solution of L1 (54.6 mg, 0.19 mmol) in MeCN (5 mL) and stirred resulting in a dark red solution. Next, a solution of NaSC$_6$H$_4$-*p*-Cl in MeCN (formed from the addition of NaH to HSC$_6$H$_4$-*p*-Cl in THF and H_2 gas allowed to fully evolve) was added to the [Fe^{II}(L1)][ClO$_4$]$_2$ and stirred resulting in a purple solution. The solvent was concentrated, and CH_2Cl_2 was added to the reaction to facilitate the precipitation of $NaClO_4$. After filtering the solution through Celite, the filtrate was collected, concentrated, and the compound was precipitated with Et_2O and the dark purple solid was isolated.

Synthesis of [Fe^{II}(L1)(SPh-*p*-Cl)(NO)]BF$_4$ (6a). A solution of Ph_3CSNO[29] (35.2 mg, 0.12 mmol) in CH_2Cl_2 (5 mL) was added to a solution of [Fe^{II}(L1)(SPhCl)][BF$_4$] (72.0 mg, 0.13 mmol) in CH_2Cl_2 (7 mL) and stirred resulting in a dark red solution. Et_2O was added to the solution to precipitate the compound and separate the disulfide (which is soluble in Et_2O), filtered and the dark red precipitate was isolated. Selected IR bands (diamond ATR, cm^{-1}): 2042 (w, ν_{N3}), 740 (m, ν_{SC}). Electronic absorption spectrum in MeCN, λ_{max} nm (ε, M^{-1} cm^{-1}) : 329 (~45,000), 530 (~1000).

Synthesis of [Fe^{II}(L1)(SPh-*p*-Cl)(NO)]ClO$_4$ (6b). To a solution of isolated [Fe^{II}(L1)(SPhCl)][ClO$_4$] (46.3 mg, 0.079 mmol) in MeCN (5 mL) was added a solution of Ph_3CSNO (21.4 mg, 0.070 mmol) in MeCN and allowed to stir. The dark purple solution was concentrated and Et_2O was added to the solution to precipitate the compound as well as to separate the compound from the formed disulfide (which is soluble in Et_2O). Selected IR bands (diamond ATR, cm^{-1}): 1094 (s, ν_{ClO4}) 741 (m, ν_{SC}).

Synthesis of $[Fe^{II}(L1)(SCPh_3)(NO)]BF_4$ (7a). To a solution of $Fe(BF_4)_2{\cdot}6H_2O$ (53.7 mg, 0.16 mmol) in MeOH (2 mL) was added a solution of L1 (47.0 mg, 0.16 mmol) in MeOH (3 mL) and stirred resulting in a red solution. To this was added a methanolic solution of $NaSC(C_6H_5)_3$ (formed from the combination of NaH and $HSC(C_6H_5)_3$ in a THF solution and isolated) and stirred resulting in a dark red solution. The solution was concentrated and CH_2Cl_2 was added to the reaction to facilitate the precipitation of $NaBF_4$. The solution was filtered with Celite, and the filtrate was collected and concentrated. Et_2O was added to the solution to precipitate the compound and isolated. This solid (43.6 mg, 0.062 mmol) was dissolved in MeCN (5 mL) and a solution of Ph_3CSNO (18.6 mg, 0.061 mmol) was added to it and stirred resulting in a dark red solution. Et_2O was added to the solution to precipitate the compound, filtered, and the orange solid was collected. Selected IR bands (diamond ATR, cm^{-1}): 1054 (w, ν_{BF4}), 745 (m, ν_{SCPh3}).

Synthesis of $[Fe^{II}(L1)(SCPh_3)(NO)]ClO_4$ (7b). To a solution of L1 (46.3 mg, 0.16 mmol) in MeOH (3 mL) was added a solution of $Fe(ClO_4)_2{\cdot}6H_2O$ (40.1 mg, 0.16 mmol) in MeOH (3 mL) and stirred resulting in a dark red solution. To this solution was added a methanolic solution of $NaSCPh_3$ (0.20 mmol) (prepared from the addition of $HSCPh_3$ to NaH in THF and isolated) and stirred resulting in a dark purple solution and an orange precipitate. This solid was isolated through filtration and analyzed. The filtrate was concentrated and CH_2Cl_2 was added to facilitate the precipitation of $NaClO_4$. This suspension was filtered through Celite, and the purple filtrate was concentrated and Et_2O was added to precipitate the compound. The dark purple solid was collected via filtration. This solid (39.3 mg, 0.055 mmol) was dissolved in MeCN, and a solution of Ph_3CSNO (15.0 mg, 0.049 mmol) in MeCN (3 mL) was added and stirred resulting in a dark purple solution. Et_2O was added to the solution, and the purple solid was isolated through filtration. Selected IR bands (diamond ATR, cm^{-1}): 1738 (w, ν_{NO}), 1095 (s, ν_{ClO4}), 741 (s, ν_{SCPh3}). Electronic absorption spectrum in MeCN, λ_{max} nm (ε, M^{-1} cm^{-1}) : 309 (~50,000) , 495 (~1500).

Synthesis of [Fe^{II}(L1)(SPhCl)(CN)]. A solution of $(Et_4N)(CN)$ (20.3 mg, 0.13 mmol) in CH_2Cl_2 (5 mL) was added to a solution of [Fe^{II}(L1)(SPhCl)][BF_4] (0.17 mmol) in CH_2Cl_2 (7 mL) and stirred resulting in a dark purple solution depositing a purple precipitate. This precipitate was isolated and characterized. Selected IR bands (diamond ATR, cm^{-1}): 2074 (w, ν_{CN}), 743 (m, ν_{SC}). Electronic absorption spectrum in MeCN, λ_{max} nm (ε, M^{-1} cm^{-1}) : 322 (~45,000), 530 (~1000).

Synthesis of [Fe^{II}(L1)(SPhCl)(N_3)]. A solution of [*n*Bu_4N][N_3] (2.7 mg, 9.5 μmol) in MeCN (5 mL) was added to a solution of [Fe^{II}(L1)(SPhCl)][BF_4] (5.7 mg, 10.0 μmol) in MeCN (7 mL) and stirred. Immediately following the addition of the azide, a purple precipitate formed. This solid was isolated and characterized. Selected IR bands (diamond ATR, cm^{-1}): 2042 (w, ν_{N3}), 740 (m, ν_{SC}). Electronic absorption spectrum in MeCN, λ_{max} nm (ε, M^{-1} cm^{-1}) : 329 (~45,000), 530 (~1000).

CHAPTER 3

SYNTHETIC ANALOGS CONTAINING IMIDAZOLE RINGS

Introduction

In the study presented herein, we have synthesized and characterized a synthetic analog more closely mimicking the planar geometry present in the active site of SOR than the previously discussed N_4 system in Chapter 2. The active site of SOR contains four histidine ligands in the equatorial plane about the iron ion. The planar imidazole N-donor geometry ligated to the iron ion in SOR contributes to its catalytic cycle, and we attempt to recreate this imidazole ligation by incorporating two imidazole rings into the planar N_4 ligand system. This ligand will promote a rigidly planar environment about the iron center.

Synthesis of Ligand (L2 and L3)

The synthesis of 1,2-bis(2'-imidazole-methyleneimino)benzene (**L2**), the neutral N_4 ligand containing imidazole donors, was attempted in order to more closely mimic the histidine ligands present in the enzyme (Scheme 3.1). The attempted synthesis was similar to the previously discussed ligand **L1** in chapter 2. However, the 2-imidazole-carboxaldehyde starting material was highly insoluble in commonly used solvents at room temperature. Upon heating the suspension of the starting material, the starting material partially dissolved, and the suspension was refluxed for four hours affording a light yellow precipitate. The collected precipitate was highly insoluble in all available solvents; therefore, the ^{1}H NMR, ^{13}C NMR, and UV-visible characterization were unobtainable, and the formation of **L2** could not be confirmed.

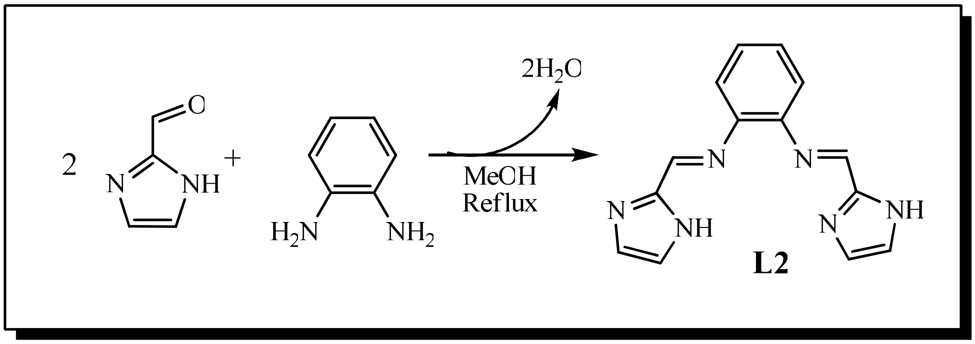

Scheme 3.1. The attempted synthesis of 1,2-bis(2'-imidazole-methyleneimino)benzene (**L2**) in MeOH.

The synthesis of (*N*^{1}E,*N*^{2}*E*)-4,5-dimethyl-*N*1,*N*2-bis((1-methyl-1H-imidazol-2-yl)methylene)benzene-1,2-diamine (**L3**) involved a Schiff base reaction with one molar equivalent of 4,5-dimethyl-1,2-phenylenediamine and two molar equivalents of 1-methyl-2-imidazolecarboxaldehyde in ethanol (EtOH) similar to the synthesis of **L1** as shown in scheme 3.2. The methyl substituents on the imidazole ring allowed for increased solubility when compared to the attempted synthesis of **L2**. The synthesis included refluxing the ethanolic solution for 16 h., and the solvent was removed in vacuo resulting in a dark orange oil which was dissolved in CH_2Cl_2. A 5% NaOH (aq) solution was then added to the solution and allowed to stir for 1 h. The CH_2Cl_2 layer was then separated and washed with saturated NaCl solution, dried over anhydrous $MgSO_4$, filtered, and the solvent was evaporated to afford a yellow oil. A 10 mL portion of MeCN was added to the oil and the mixture stirred for ~ 1 h resulting in the precipitation of a light yellow solid. This solid was collected and an additional base wash as described earlier was performed resulting in a solid that was stored under an N_2 atmosphere before being used. The formation of **L3** was confirmed by ^{1}H NMR, and the solid-state FTIR spectrum of **L3** was obtained (Figure 3.1).

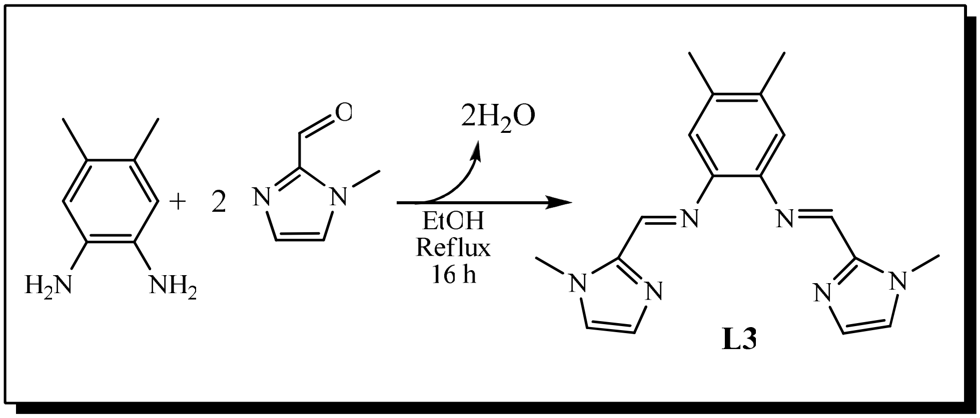

Scheme 3.2. The synthesis of the neutral imidazole(N)-donor ligand **L3**.

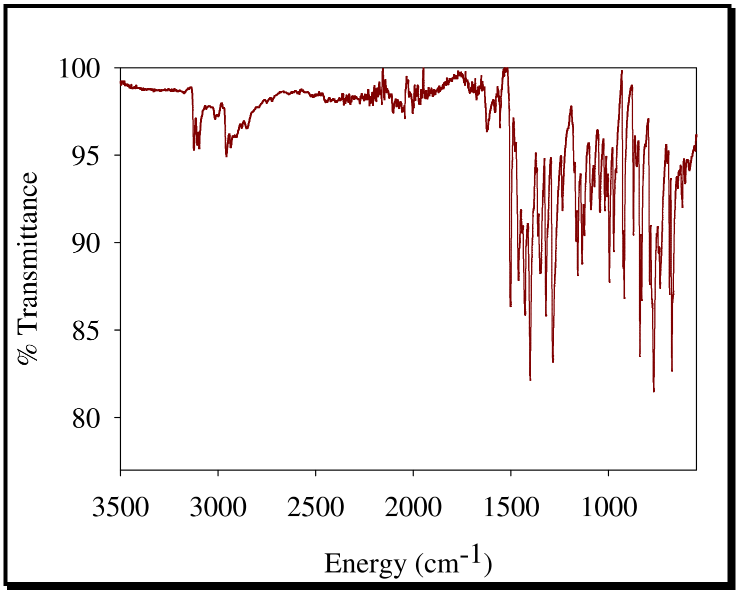

Figure 3.1. Solid-state FTIR of **L3** (ATR).

Preparation and Characterization of Fe Complexes

The synthesis of $[Fe^{II}(L3)](BF_4)_2$ (**10**) was attempted by following a procedure similar to the synthesis of compound **3** discussed previously in chapter 2. One molar equivalent of $[Fe(H_2O)](BF_4)_2$ in MeCN was added to a suspension of **L3** in MeCN resulting in a dark green solution (Scheme 3.3). Upon taking the ESI-MS of this reaction mixture, the *m/z* corresponding to the compound **10** was present as well as an additional *m/z* corresponding to $[Fe(L3)_2]^{2+}$ (**11**). Upon removing the solvent and dissolving the remaining material in DMF, Et_2O was diffused into the solution and blue-green crystals formed. When the crystal structure was solved via X-ray analysis, it was determined that the crystals formed were the eight-coordinate species $[Fe(L3)_2](BF_4)_2$ with four imine nitrogen atoms and four imidazole nitrogen atoms bound to the ferrous center in a square-anitprism coordination geometry (Figure 3.5). The electron-donating effects of this compound were investigated through the variation of the substituents on the benzene ring.[84] Since **L3** contain methyl groups as the substituents, this ligand was used as the electron-donating ligand among the chelating ligands utilized. The effects of the electron-donating ability were observed via electrochemical analysis as well as electronic absorption spectroscopy. The cyclic voltammetry revealed the relative effects of the different ligand substituents with compound **11** having a reversible Fe^{2+}/Fe^{3+} couple at $E_{1/2} = 0.395$ V (vs Ag/AgCl, MeCN) (Figure 3.2) that was the least positive when compared to ligands containing H and Cl^- as the substituents on the benzene ring. This is to be expected since the methyl substituents on the benzene ring would be provide the most electron density to the iron center resulting in the relative ease of oxidation. The compound containing hydrogen as its substituent was found to be unaffected by air as well as other chemical oxidizing agents and strong field ligands, but similar experiments were not analyzed with **11.** The electronic absorption spectrum of **11** in an MeCN solution exhibits two indicative peaks for the 8-coordinate systems at 319 nm ($\varepsilon = 26300\ M^{-1}cm^{-1}$) and 387 nm ($\varepsilon = 13,900\ M^{-1}cm^{-1}$) with a shoulder at 333 nm ($\varepsilon = 20900\ M^{-1}cm^{-1}$) (Figure 3.3). The higher concentration spectrum at 170 μM solution shows a peak at 546 nm (ε 380 $M^{-1}cm^{-1}$) with a shoulder at 661 nm (ε 280 $M^{-1}cm^{-1}$) likely arising from a d-d transition. The FTIR spectrum of the 8-coordinate compound **11** was acquired and exhibits a B-F stretch attributing to the presence of two BF_4^- counteranions (Figure 3.4). Although **11** is a novel compound, it proves to be very stable and not useful for the purposes of modeling SOR.

However, **11** demonstrates the rigidity of **L3** which is useful to maintain the necessary SOR modeling square-pyramidal geometry when the $[Fe(L3)]^{2+}$ is successfully isolated.

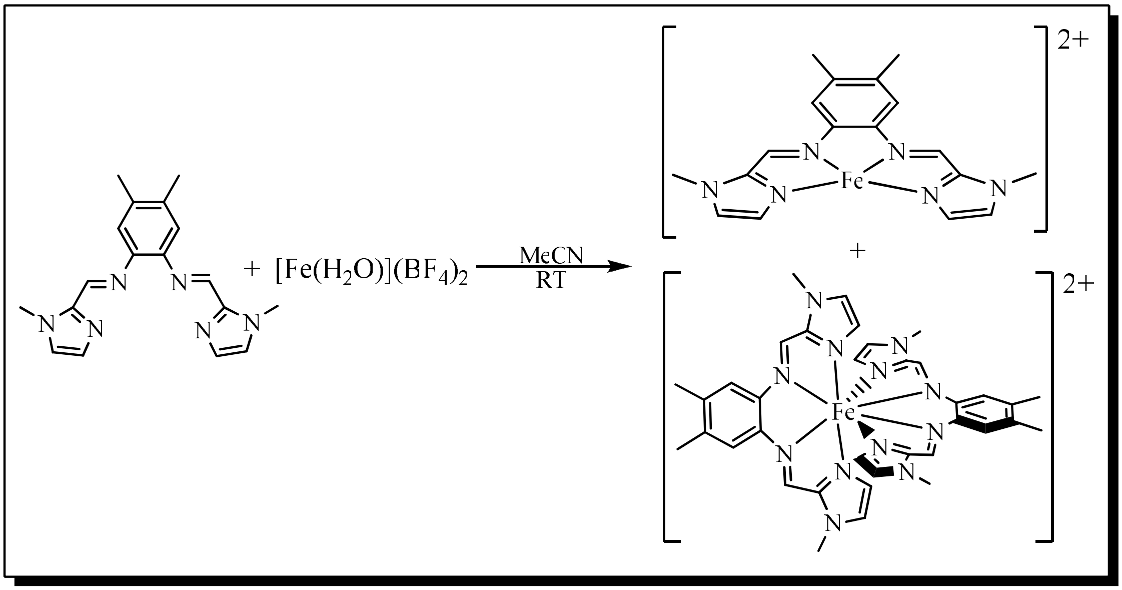

Scheme 3.3. The reaction of L3 with $[Fe(H_2O)](BF_4)_2$ resulting in $[Fe(L3)]^{2+}$ (**10**) and $[Fe(L3)_2]^{2+}$ (**11**).

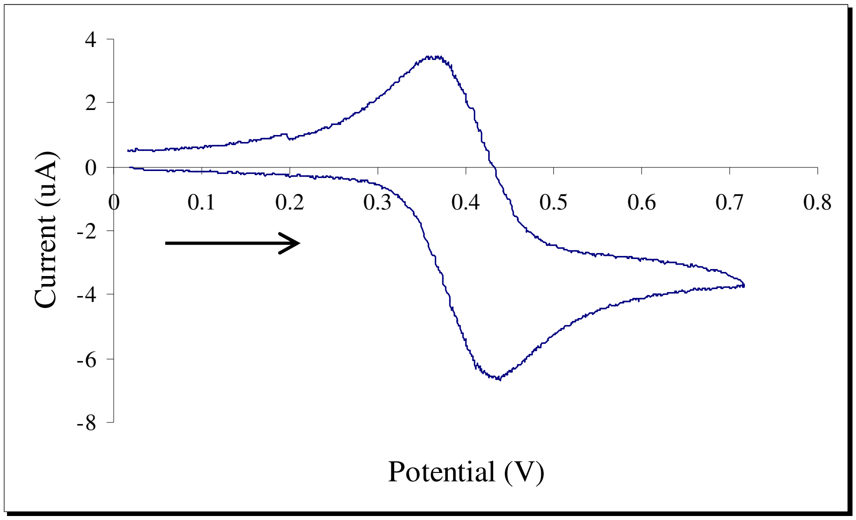

Figure 3.2. Cyclic voltammogram of **11**. $E_{1/2} = 0.395$ V (versus Ag/AgCl in MeCN with 0.1 M ${}^{t}Bu_4NPF_6$ supporting electrolyte, glassy carbon working electrode, Pt-wire auxiliary electrode, scan rate 50 mV/s, RT)

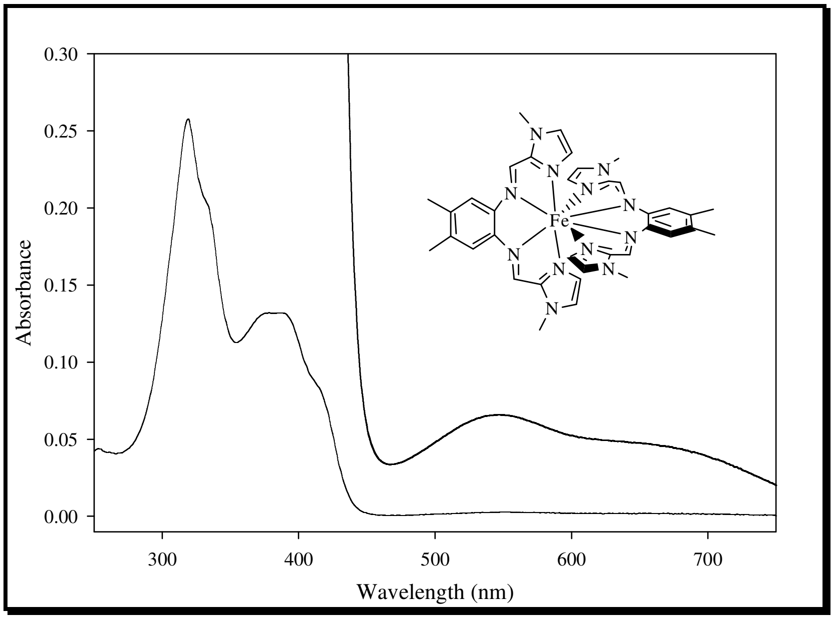

Figure 3.3. UV-vis spectrum of the 8-coordinate species $[Fe(L3)_2](BF_4)_2$ (**11**) in MeCN at 298 K.

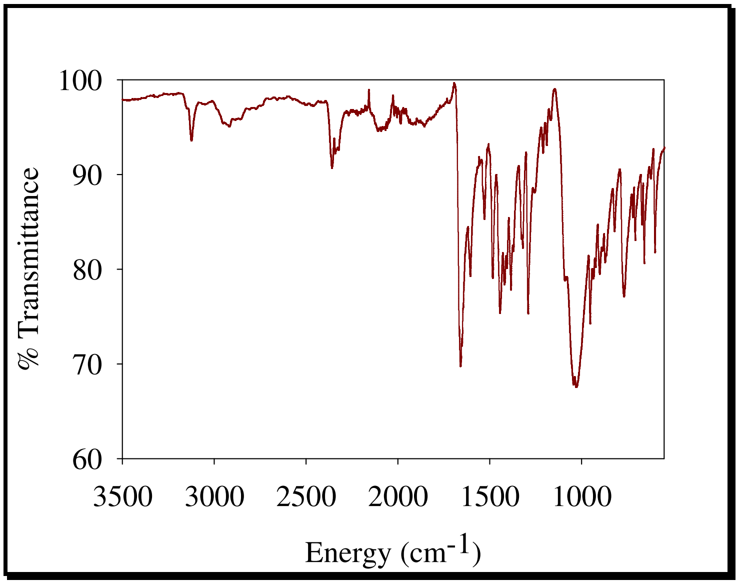

Figure 3.4. Solid-state FTIR spectrum of compound **11** with BF_4^- band present (ATR).

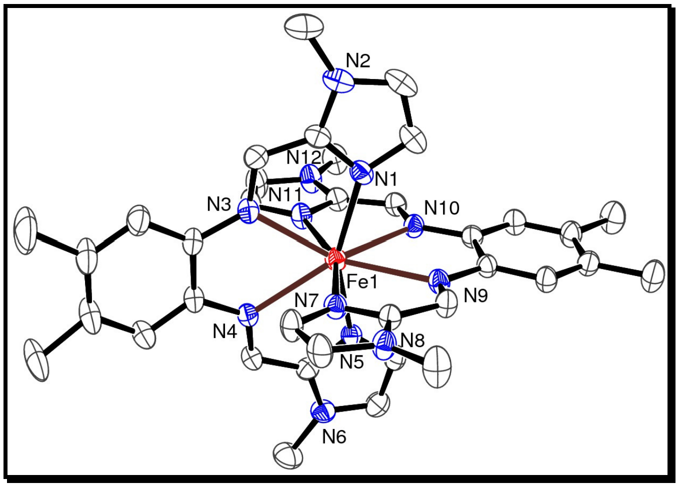

Figure 3.5. ORTEP diagrams of the cationic complex $[Fe(L2)_2](BF_4)_2$ (**11**) showing 30% thermal ellipsoids for all non-hydrogen atoms.

Table 3.1. Summary of crystal data and intensity collection and structure refinement parameters for $[Fe(L3)_2](BF_4)_2$•DMF (**11**•DMF).

Parameters	**11**•DMF
Formula	$C_{39}H_{47}N_{13}OB_2F_8Fe$
Formula weight	943.37
Crystal system	Triclinic
Space group	*P*-1
Crystal color, habit	green rhombic
a, Å	12.322(5)
b, Å	12.468(5)
c, Å	16.367(5)
α, deg	77.860(5)
β, deg	86.532(5)
γ, deg	88.057(5)
V, Å^3	2453.2(16)
Z	2
ρ_{calcd}, g/cm^{-3}	1.277
T, K	293(2)
abs coeff, μ (Mo Kα), mm^{-1}	0.382
θ limits, deg	2.30-28.29
total no. of data	33446
no. of unique data	12053
no. of parameters	577
GOF on F^2	0.967
R_1,[a] %	6.79
wR_2,[b] %	19.34
max, min peaks, e/Å^3	0.938, -0.600

[a] $R_1 = \Sigma||F_o| - |F_c|| / \Sigma|F_o|$; [b] $wR_2 = \{\Sigma[w(F_o^2 - F_c^2)^2]/\Sigma[w(F_o^2)^2]\}^{1/2}$.

Table 3.2. Selected bond distances (Å) and bond angles (deg) for $[Fe(L_3)_2](BF_4)_2$•DMF (**11**•DMF).

Fe(1)-N(1)	2.236(2)	N(1)-Fe(1)-N(4)	132.29(7)	N(3)-Fe(1)-N(9)	134.26(7)
Fe(1)-N(3)	2.505(2)	N(1)-Fe(1)-N(5)	158.14(8)	N(3)-Fe(1)-N(10)	137.70(7)
Fe(1)-N(4)	2.483(2)	N(1)-Fe(1)-N(7)	92.81(8)	N(3)-Fe(1)-N(11)	77.45(8)
Fe(1)-N(5)	2.241(2)	N(1)-Fe(1)-N(9)	79.84(8)	N(4)-Fe(1)-N(5)	69.53(7)
Fe(1)-N(7)	2.225(2)	N(1)-Fe(1)-N(10)	82.52(7)	N(4)-Fe(1)-N(7)	79.00(7)
Fe(1)-N(9)	2.428(2)	N(1)-Fe(1)-N(11)	88.09(8)	N(4)-Fe(1)-N(9)	136.81(7)
Fe(1)-N(10)	2.398(2)	N(3)-Fe(1)-N(4)	63.10(7)	N(4)-Fe(1)-N(10)	134.51(7)
Fe(1)-N(11)	2.214(2)	N(3)-Fe(1)-N(5)	132.55(7)	N(4)-Fe(1)-N(11)	81.04(7)
N(1)-Fe(1)-N(3)	69.20(7)	N(3)-Fe(1)-N(7)	78.36(7)	N(5)-Fe(1)-N(7)	90.50(8)
N(5)-Fe(1)-N(9)	80.98(8)	N(7)-Fe(1)-N(9)	70.20(8)	N(9)-Fe(1)-N(10)	65.45(7)
N(5)-Fe(1)-N(10)	80.03(7)	N(7)-Fe(1)-N(10)	135.54(8)	N(9)-Fe(1)-N(11)	135.50(8)
N(5)-Fe(1)-N(11)	98.36(8)	N(7)-Fe(1)-N(11)	153.73(8)	N(10)-Fe(1)-N(11)	70.61(7)

Conclusion

The synthesis of **L3** afforded a ligand similar to the histidine equatorial plane of the active site of SOR. The reaction of **L3** with $[Fe(H_2O)_6](BF_4)_2$ produced novel results affording an eight-coordinate system with two nitrogenous ligands about an Fe^{2+} ion. Although preliminary data has only been obtained with this system, the electron-donating effects of this ligand have been determined and may be useful in tuning the electronic characteristics of an SOR analog by varying the N-donor strength of the N_4 ligand. The rigidly planar ligand frame provides evidence for the utilization of **L3** as the planar N_4 system in an SOR model will be an optimum ligand mimicking the structural properties of SOR. Further studies of the reaction of **L3** with a different iron salt, such as $FeCl_2$, will elucidate the formation of $[Fe(L3)]^{2+}$.

Experimental Section

The general procedures and physical methods used are analogous to those presented in Chapter 2.

(*N*^{1}E,*N*^{2}*E*)-4,5-dimethyl-*N*1,*N*2-bis((1-methyl-1H-imidazol-2-yl)methylene)benzene-1,2-diamine (L3). To a solution of 4,5-dimethyl-1,2-phenylenediamine (0.520 g, 3.82 mmol) in 10 mL EtOH was added a solution of 1-methyl-2-imidazolecarboxaldehyde (0.860 g, 7.81 mmol) in 5 mL of EtOH and the solution was refluxed for 16 h. The solvent was removed in vacuo resulting in a dark orange oil which was dissolved in CH_2Cl_2. A 5% NaOH (aq) solution was then added to the solution and allowed to stir for 1 h. The CH_2Cl_2 layer was then separated, washed with saturated NaCl solution, dried over anhydrous $MgSO_4$, filtered and the solvent was evaporated to afford a yellow oil. A 10 mL portion of MeCN was added to the oil and the mixture stirred for ~ 1 h resulting in the precipitation of a light yellow solid. This solid was collected and an additional base wash analogous to the previous was performed on the solid in order to extract the carboxaldehyde starting material. The CH_2Cl_2 was removed and the solid was collected to afford a yellow solid. ^{1}H NMR (400 MHz, $CDCl_3$, δ from TMS, 298 K): 8.53 (s, 2H), 7.30 (s, 2H), 7.16 (d, 2H), 6.94 (d, 2H), 3.90 (s, 6H), 2.35 (s, 6H). ^{13}C NMR (100.6 MHz, $CDCl_3$, δ): 153 (*C*H=N), 141.45 (Ar-*C*), 126.41 (Ar-*C*), 125.72 (Ar-*C*), 122.19 (Ar-*C*), 120.44 (Ar-*C*), 117.92 (Ar-*C*), 109.95 (Ar-*C*), 41.03 (N-*C*H$_3$), 18.43 (Ar-*C*H$_3$). FTIR (ATR-diamond, powder) ν_{max} (cm^{-1}): 1605 (w, $\nu_{C=N}$), 1469 (m), 1445 (m), 1268 (m), 1157 (m), 952 (m), 843 (s), 646 (w), 616 (s). LRMS-ESI (*m/z*): $[M + H]^+$ calcd. for $C_{18}H_{21}N_6$, 321.2; found, 321.0.

$[Fe(L3)_2](BF_4)_2$ (11). To a suspension of L3 (0.534 g, 1.67 mmol) in MeCN was added a solution of $[Fe(H_2O)_6](BF_4)_2$ (0.561 g, 1.66 mmol) in MeCN resulting in a dark green solution. The solvent was removed in vacuo and the solvent was redissolved in 5 mL of DMF. Vapor diffusion of Et_2O into this solution at RT resulted in the formation of dark blue-green crystalline material after approximately 18 h. This crystal was determined to be the eight-coordinate species, $[Fe(L_3)_2](BF_4)_2$ (**11**). Upon further vapor diffusion of Et_2O into the DMF solution more microcrystalline material formed (0.20 g, 0.29 mmol, 28%) FTIR (ATR-diamond, solid), ν_{max} (cm^{-1}): 1606 (w, $\nu_{C=N}$), 1659 (s), 1444 (m), 1291 (w), 1030 (vs, BF_4^-), 953 (m), 821 (w), 769 (m), 658 (w), 599 (m). UV-vis (MeCN), λ_{max}, nm (ε, M^{-1} cm^{-1}): 319 (26,300), 333sh (20,900), 387 (13,900), 546 (390), 647 (280). LRMS-ESI (*m/z*): $[M - 2\ BF_4]^{2+}$ calcd for $C_{36}H_{40}FeN_{12}$, 348.1; found, 348.2. $\mu_{eff} = 4.45\ \mu_B$ (in MeCN). $E_{1/2}$ ($Fe^{II/III}$, MeCN): 0.395 V. Anal. Calcd for $C_{36}H_{40}B_2F_8FeN_{12}$: C, 49.69; H, 4.63; N, 19.31. Found: C, 47.93; H, 4.91; N, 18.00.

REFERENCES

1. Castilla, P.; Davalos, A.; Teruel, J. L.; Cerrato, F.; Fernandez-Lucas, M.; Merino, J. L.; Sanchez-Martin, C. C.; Ortuno, J.; Lasuncion, M. A., *Am. J. Clin. Nutr.* **2008,** *87*, 1053-1061.

2. Roy, S. C.; Atreja, S. K., *Animal Reproduction Science* **2008,** *103*, 260-270.

3. Mueller, C. F. H.; Laude, K.; McNally, J. S.; Harrison, D. G., *Arterioscler., Thromb., Vasc. Biol.* **2005,** *25*, 274-278.

4. Valentine, J. S.; Wertz, D. L.; Lyons, T. J.; Liou, L.-L.; Goto, J. J.; Gralla, E. B., *Curr. Op. Chem. Biol.* **1998,** *2*, 253-262.

5. Park, J.-W.; Babior, B. M., *Biochemistry* **1997,** *36*, 7474-7480.

6. Irani, K.; Xia, Y.; Zweier, J. L.; Sollott, S. J.; Der, C. J.; Fearon, E. R.; Sundaresan, M.; Finkel, T.; Goldschmidt-Clermont, P. J., *Science* **1997,** *275*, 1649-1652.

7. Sundaresan, M.; Yu, Z.-X.; Ferrans, V. J.; Irani, K.; Finkel, T., *Science* **1995,** *270*, 296-299.

8. Kroemer, G.; Zamzami, N.; Susin, S. A., *Immunology Today* **1997,** *18*, 44-51.

9. Polyak, K.; Xia, Y.; Zweier, J. L.; Kinzler, K. W.; Vogelstein, B., *Nature* **1997,** *389*, 300-305.

10. Dean, R. T.; Fu, S.; Stocker, R.; Davies, M. J., *Biochem. J.* **1997,** *324*, 1-18.

11. Henle, E. S.; Linn, S., *J. Biol. Chem.* **1997,** *272*, 19095-19098.

12. Steinberg, D., *J. Biol. Chem.* **1997,** *272*, 20963-20966.

13. Albertini, R.; Moratti, R.; De Luca, G., *Curr. Mol. Med.* **2002,** *2*, 579-592.

14. Grune, T., Ed., *Free Radicals and Diseases: Gene Expression, Cellular Metabolism and Pathophysiology*. IOS Press: Amsterdam; Oxford; Washington, DC, 2005; Vol. 367.

15. Hattori, Y.; Kawasaki, H.; Abe, K.; Kanno, M., *Am. J. Physiol.* **1991,** *261*, H1086-H1094.

16. Muller, F., *J. Am. Aging Assoc.* **2000,** *23*, 227-253.

17. Ohara, Y.; Peterson, T. E.; Harrison, D. G., *J. Clin. Invest.* **1993,** *91*, 2546-51.

18. Rajagopalan, S.; Kurz, S.; Muenzel, T.; Tarpey, M.; Freeman, B. A.; Griendling, K. K.; Harrison, D. G., *J. Clin. Invest.* **1996,** *97*, 1916-23.

19. Rubanyi, G. M.; Vanhoutte, P. M., *Am. J. Physiol. Heart Circ. Physiol.* **1986,** *250*, H822-827.

20. Heistad, D. D., *Arterioscler Thromb Vasc Biol* **2006,** *26*, 689-695.

21. McCord, J. M.; Fridovich, I., *J. Biol. Chem.* **1969,** *244*, 6049-6055.

22. Chance, B.; Sies, H.; Boveris, A., *Physiol. Rev.* **1979,** *59*, 527-605.

23. Fridovich, I., *Annu. Rev. Biochem.* **1995,** *64*, 97-112.

24. Wuerges, J.; Lee, J.-W.; Yim, Y.-I.; Yim, H.-S.; Kang, S.-O.; Carugo, K. D., *Proc. Natl. Acad. Sci. U.S.A.* **2004,** *101*, 8569-8574.

25. Halliwell, B.; Gutteridge, J. M. C., *Free Radicals in Biology and Medicine*. Oxford University Press: New York: 1999.

26. Realini, L.; De Ridder, K.; Palomino, J. C.; Hirschel, B.; Portaels, F., *J. Clin. Microbiol.* **1998,** *36*, 2565-2570.

27. Kurtz, D.; Coulter, E., *J. Biol. Inorg. Chem.* **2002,** *7*, 653-658.

28. Imlay, J., *J. Biol. Inorg. Chem.* **2002,** *7*, 659-663.

29. Jenney, F. E., Jr.; Verhagen, M. F.; Cui, X.; Adams, M. W. W., *Science* **1999,** *286*, 306-309.

30. Adams, M. W. W.; Jenney, F. E.; Clay, M. D.; Johnson, M. K., *J. Biol. Inorg. Chem.* **2002,** *7*, 647-652.

31. Nivière, V.; Fontecave, M., *J. Biol. Inorg. Chem.* **2004,** *9*, 119-123.

32. Abreu, I.; Xavier, A.; LeGall, J.; Cabelli, D.; Teixeira, M., *J. Biol. Inorg. Chem.* **2002,** *7*, 668-674.

33. Brines, L. M.; Kovacs, J. A., *Eur. J. Inorg. Chem.* **2007,** *2007*, 29-38.

34. Yeh, A. P.; Hu, Y.; Jenney, F. E.; Adams, M. W. W.; Rees, D. C., *Biochemistry* **2000,** *39*, 2499-2508.

35. Coelho, A. V.; Matias, P.; Fülöp, V.; Thompson, A.; Gonzalez, A.; Carrondo, M. A., *J. Biol. Inorg. Chem.* **1997,** *2*, 680-689.

36. Clay, M. D.; Jenney, F. E.; Noh, H. J.; Hagedoorn, P. L.; Adams, M. W. W.; Johnson, M. K., *Biochemistry* **2002,** *41*, 9833-9841.

37. Clay, M. D.; Yang, T.-C.; Jenney, Francis E.; Kung, I. Y.; Cosper, C. A.; Krishnan, R.; Kurtz, Donald M.; Adams, M. W. W.; Hoffman, B. M.; Johnson, M. K., *Biochemistry* **2006,** *45*, 427-438.

38. Emerson, J. P.; Cabelli, D. E.; Kurtz, D. M., *Proc. Natl. Acad. Sci. U.S.A.* **2003,** *100*, 3802-3807.

39. Clay, M. D.; Emerson, J. P.; Coulter, E. D.; Kurtz, D. M., Jr.; Johnson, M. K., *J. Biol. Inorg. Chem.* **2003,** *8*, 671-682.

40. Halfen, J. A.; Moore, H. L.; Fox, D. C., *Inorg. Chem.* **2002,** *41*, 3935-3943.

41. Yang, T.-C.; McNaughton, R. L.; Clay, M. D.; Jenney, F. E.; Krishnan, R.; Kurtz, D. M.; Adams, M. W. W.; Johnson, M. K.; Hoffman, B. M., *J. Am. Chem. Soc.* **2006,** *128*, 16566-16578.

42. Dey, A.; Jenney, F. E.; Adams, M. W. W.; Johnson, M. K.; Hodgson, K. O.; Hedman, B.; Solomon, E. I., *J. Am. Chem. Soc.* **2007,** *129*, 12418-12431.

43. Emerson, J. P.; Coulter, E. D.; Cabelli, D. E.; Phillips, R. S.; Kurtz, D. M., *Biochemistry* **2002,** *41*, 4348-4357.

44. Lombard, M.; Houee-Levin, C.; Touati, D.; Fontecave, M.; Niviere, V., *Biochemistry* **2001,** *40*, 5032-5040.

45. Grunden, A. M.; Jenney, F. E., Jr.; Ma, K.; Ji, M.; Weinberg, M. V.; Adams, M. W. W., *Appl. Environ. Microbiol.* **2005,** *71*, 1522-1530.

46. Katona, G.; Carpentier, P.; Niviere, V.; Amara, P.; Adam, V.; Ohana, J.; Tsanov, N.; Bourgeois, D., *Science* **2007,** *316*, 449-453.

47. Coulter, E. D.; Emerson, J. P.; Kurtz, D. M.; Cabelli, D. E., *J. Am. Chem. Soc.* **2000,** *122*, 11555-11556.

48. Abreu, I. A.; Saraiva, L. M.; Soares, C. M.; Teixeira, M.; Cabelli, D. E., *J. Biol. Chem.* **2001,** *276*, 38995-39001.

49. Clay, M. D.; Jenney, F. E.; Hagedoorn, P. L.; George, G. N.; Adams, M. W. W.; Johnson, M. K., *J. Am. Chem. Soc.* **2002,** *124*, 788-805.

50. Sawyer, D. T.; Valentine, J. S., *Acc. Chem. Res.* **1981,** *14*, 393-400.

51. Nivière, V.; Asso, M.; Weill, C. O.; Lombard, M.; Guigliarelli, B.; Favaudon, V.; Houee-Levin, C., *Biochemistry* **2004,** *43*, 808-818.

52. Clay, M. D.; Cosper, C. A.; Jenney, F. E.; Adams, M. W. W.; Johnson, M. K., *Proc. Natl. Acad. Sci. U.S.A.* **2003,** *100*, 3796-3801.

53. Enemark, J. H.; Feltham, R. D., *Coord. Chem. Rev.* **1974,** *13*, 339-406.

54. Brown, C. A.; Pavlosky, M. A.; Westre, T. E.; Zhang, Y.; Hedman, B.; Hodgson, K. O.; Solomon, E. I., *J. Am. Chem. Soc.* **1995,** *117*, 715-732.

55. Westre, T. E.; Di Cicco, A.; Filipponi, A.; Natoli, C. R.; Hedman, B.; Solomon, E. I.; Hodgson, K. O., *J. Am. Chem. Soc.* **1994,** *116*, 6757-6768.

56. Fiedler, A. T.; Halfen, H. L.; Halfen, J. A.; Brunold, T. C., *J. Am. Chem. Soc.* **2005,** *127*, 1675-1689.

57. Namuswe, F.; Kasper, G. D.; Sarjeant, A. A. N.; Hayashi, T.; Krest, C. M.; Green, M. T.; Moenne-Loccoz, P.; Goldberg, D. P., *J. Am. Chem. Soc.* **2008,** *130*, 14189-14200.

58. Addison, A. W.; Rao, T. N.; Reedijk, J.; Rijn, J. V.; Verschoor, G. C., *J. Chem. Soc., Dalton Trans.* **1984**, 1349-1356.

59. Bukowski, M. R.; Koehntop, K. D.; Stubna, A.; Bominaar, E. L.; Halfen, J. A.; Munck, E.; Nam, W.; Que, L., Jr., *Science* **2005,** *310*, 1000-1002.

60. Kovacs, J. A.; Brines, L. M., *Acc. Chem. Res.* **2007,** *40*, 501-509.

61. Kitagawa, T.; Dey, A.; Lugo-Mas, P.; Benedict, J. B.; Kaminsky, W.; Solomon, E.; Kovacs, J. A., *J. Am. Chem. Soc.* **2006,** *128*, 14448-14449.

62. Roelfes, G.; Vrajmasu, V.; Chen, K.; Ho, R. Y. N.; Rohde, J.-U.; Zondervan, C.; la Crois, R. M.; Schudde, E. P.; Lutz, M.; Spek, A. L.; Hage, R.; Feringa, B. L.; Munck, E.; Que, L., *Inorg. Chem.* **2003,** *42*, 2639-2653.

63. Namuswe, F.; Kasper, G. D.; Sarjeant, A. A. N.; Hayashi, T.; Krest, C. M.; Green, M. T.; Moenne-Loccoz, P.; Goldberg, D. P., *J. Am. Chem. Soc.* **2008,** *130*, 14189-14200.

64. Krishnamurthy, D.; Kasper, G. D.; Namuswe, F.; Kerber, W. D.; Narducci Sarjeant, A. A.; Moenne-Loccoz, P.; Goldberg, D. P., *J. Am. Chem. Soc.* **2006,** *128*, 14222-14223.

65. Emerson, J. P.; Farquhar, E. R.; Que, L. J., *Angew. Chem., Int. Ed.* **2007,** *46*, 8553-8556.

66. Lehnert, N.; Ho, R. Y. N.; Que, Lawrence; Solomon, E. I., *J. Am. Chem. Soc.* **2001,** *123*, 8271-8290.

67. Bukowski, M. R.; Halfen, H.; van den Berg, T. A.; Halfen, J. A.; Que, L. J., *Angew. Chem., Int. Ed.* **2005,** *44*, 584-587.

68. Shearer, J.; Nehring, J.; Lovell, S.; Kaminsky, W.; Kovacs, J. A., *Inorg. Chem.* **2001,** *40*, 5483-5484.

69. Shearer, J.; Scarrow, R. C.; Kovacs, J. A., *J. Am. Chem. Soc.* **2002,** *124*, 11709-11717.

70. Theisen, R. M.; Shearer, J.; Kaminsky, W.; Kovacs, J. A., *Inorg. Chem.* **2004,** *43*, 7682.

71. Spyridoula, K.; Achilleas, G.; George, K.; Spyros, P. P.; Nick, H., *Transition Met. Chem.* **1993,** *18*, 531-536.

72. Mishra, D.; Naskar, S.; Butcher, R. J.; Chattopadhyay, S. K., *Inorg. Chim. Acta* **2005,** *358*, 3115-3121.

73. Kasselouri, S., *J. Coord. Chem.* **1998,** *44*, 55 - 59.

74. Garoufis, A.; Kasselouri, S.; Mitsopoulou, C.-A.; Sletten, J.; Papadimitriou, C.; Hadjiliadis, N., *Polyhedron* **1998,** *18*, 39-47.

75. Clay, M. D.; Cosper, C. A.; Jenney, F. E., Jr.; Adams, M. W. W.; Johnson, M. K., *Proc. Natl. Acad. Sci. U. S. A.* **2003,** *100*, 3796-3801.

76. Shepherd, R. E.; Sweetland, M. A.; Junker, D. E., *J. Inorg. Biochem.* **1997,** *65*, 1-14.

77. Lippard, S. J.; Berg, J. M., *Principles of Bioinorganic Chemistry*. University Science Books: Mill Valley, CA, 1994.

78. Dickson, D. P. E.; Berry, F. J., *Mössbauer Spectroscopy*. Cambridge University: New York, 1986.

79. Urbansky, E. T., *Bioremediation Journal* **1998,** *2*, 81 - 95.

80. King, W. R. J.; Garner, C. S., *J. Phys. Chem.* **1954,** *58*, 29-33.

81. Pan, Z.; Wang, Q.; Sheng, X.; Horner, J. H.; Newcomb, M., *J. Am. Chem. Soc.* **2009,** *131*, 2621-2628.

82. Al-Mustafa, J. I., *Vibrational Spectroscopy* **2002,** *30*, 139-146.

83. Tom, R. T.; Samal, A. K.; Sreeprasad, T. S.; Pradeep, T., *Langmuir* **2006,** *23*, 1320-1325.

84. Patra, A. K.; Cheatum, W. H.; Dube, K.; Harrop, T., *unpublished results*.